

A census of molecular hydrogen outflows and their sources along the Orion A molecular ridge

Characteristics and overall distribution

C.J. Davis¹, D. Froebrich², T. Stanke³, S.T. Megeath⁴, M.S.N. Kumar⁵, A. Adamson¹, J. Eisloffel⁶, R. Gredel⁷,
T. Khanzadyan⁸, P. Lucas⁹, M.D. Smith² and W.P. Varricatt¹

¹ Joint Astronomy Centre, 660 North A'ohökü Place, University Park, Hilo, Hawaii 96720, U.S.A.
e-mail: c.davis@jach.hawaii.edu

² Centre for Astrophysics & Planetary Science, School of Physical Sciences, University of Kent, Canterbury CT2 7NR, U.K.

³ European Southern Observatory, Garching, Germany

⁴ Department of Physics and Astronomy, University of Toledo, Toledo, OH 43606-3390, U.S.A.

⁵ Centro de Astrofísica da Universidade do Porto, Rua das Estrelas s/n 4150-762 Porto, Portugal

⁶ Thüringer Landessternwarte Tautenburg, Sternwarte 5, D-07778 Tautenburg, Germany

⁷ Max Plank Institute für Astronomie, Königstuhl 17, D-69117 Heidelberg, Germany

⁸ Centre for Astronomy, Department of Experimental Physics, National University of Ireland, Galway, Ireland

⁹ Centre for Astrophysics Research, Science & Technology Research Institute, University of Hertfordshire, College Lane, Hatfield AL10 9AB, U.K.

Received: October 1, 2008. Accepted: ...

Abstract.

Aims. A census of molecular hydrogen flows across the entire Orion A Giant Molecular Cloud is sought. With this paper we aim to associate each flow with its progenitor and associated molecular core, so that the characteristics of the outflows and outflow sources can be established.

Methods. We present wide-field near-infrared images of Orion A, obtained with the Wide Field Camera, WFCAM, on the United Kingdom Infrared Telescope. Broad-band K and narrow-band H₂ 1-0S(1) images of a contiguous ~8 square degree region are compared to mid-IR photometry from the Spitzer Space Telescope and (sub)millimetre dust-continuum maps obtained with the MAMBO and SCUBA bolometer arrays. Using previously-published H₂ images, we also measure proper motions for H₂ features in 33 outflows, and use these data to help associate flows with existing sources and/or dust cores.

Results. Together these data give a detailed picture of dynamical star formation across this extensive region. We increase the number of known H₂ outflows to 116. A total of 111 H₂ flows were observed with Spitzer; outflow sources are identified for 72 of them (12 more H₂ flows have tentative progenitors). The MAMBO 1200 μ m maps cover 97 H₂ flows; 57 of them (59%) are associated with Spitzer sources and either dust cores or extended 1200 μ m emission. The H₂ jets are widely distributed and randomly orientated; the jets do not appear to be orthogonal to large-scale filaments or even to the small-scale cores associated with the outflow sources (at least when traced with the 11'' resolution of the 1200 μ m MAMBO observations). Moreover, H₂ jet lengths (L) and opening angles (θ) are not obviously correlated with indicators of outflow source age – source spectral index, α (measured from mid-IR photometry), or (sub)millimetre core flux. It seems clear that excitation requirements limit the usefulness of H₂ as a tracer of L and θ (though jet position angles are well defined).

Conclusions. We demonstrate that H₂ jet sources are predominantly protostellar sources with flat or positive near-to-mid-IR spectral indices, rather than disk-excess (or T Tauri) stars. Most protostars associated with molecular cores drive H₂ outflows. However, not all molecular cores are associated with protostars or H₂ jets. On statistical grounds, the H₂ jet phase may be marginally shorter than the protostellar phase, though must be considerably (by an order of magnitude) shorter than the prestellar phase. In terms of range and mean value of α , H₂ jet sources are indistinguishable from protostars. The spread in α observed for both protostars and H₂ outflow sources is probably a function of inclination angle as much as source age. The few true protostars without H₂ jets are almost certainly more evolved than their H₂-jet-driving counterparts, although these later stages of protostellar evolution (as the source transitions to being a “disk excess” source) must be very brief, since a large fraction of protostars do drive H₂ flows. We also find that protostars that power molecular outflows are no more (nor no less) clustered than protostars that do not. This suggests that the H₂ emission regions in jets and outflows from young stars weaken and fade very quickly, before the source evolves from protostar to pre-main-sequence star, and on time-scales much shorter than those associated with the T Tauri phase, the Herbig-Haro jet phase, and the dispersal of young stellar objects.

Key words. Stars: circumstellar matter – Infrared: ISM – ISM: jets and outflows – ISM: Herbig-Haro objects – Stars: mass-loss

1. Introduction

The southern part of the Orion constellation encompasses the Orion A and B Giant Molecular Clouds (GMCs), numerous compact and intermediate-sized molecular cores, low and high mass young stars (including a massive star/young OB cluster), stars at varying evolutionary stages, and dozens of optical Herbig-Haro (HH) objects and molecular outflows (see Peterson & Megeath (2008) and Allen & Davis (2008) for reviews). In molecular line maps the complex extends roughly northwest-southeast, parallel with the Galactic plane, over about 13° (Kutner et al. 1977; Sakamoto et al. 1994). Overall, the Orion A and B GMCs represent one of the richest star forming regions known.

In extensive regions like Orion, jets and outflows can be used as sign-posts of on-going star formation. An abundance of jets points to active accretion and a young stellar population; a paucity of molecular outflows, in a region where near- and mid-IR photometry still indicate a sizable population of sources with reddening and excess, suggests a more evolved region with a fraction of pre-main-sequence stars (T Tauri and Herbig Ae/Be stars) observed “edge-on” through their circumstellar disks.

By using H_2 2.122 μm emission as a tracer of jets and outflows, wide-field narrow-band images may be used to pin-point the locations of the youngest sources. Moreover, they allow one to take a statistical approach when considering questions about the distribution of Class 0/I protostars and Class II/III Young Stellar Objects (YSOs), the interaction of these forming stars with their surrounding environment, the overall star formation efficiency, and the evolution of the region as a whole (e.g. Stanke 2000; Stanke, McCaughrean & Zinnecker 2002; Davis et al. 2007; Kumar et al. 2007; Davis et al. 2008).

With the wide-field near-IR camera WFCAM at the United Kingdom Infrared Telescope (UKIRT) we have secured homogeneously deep, sub-arcsecond-resolution H_2 2.122 μm and broad-band K images over most of the Orion A GMC. Our ~ 8 square degree mosaics encompass the the molecular clouds known as OMC 2 and OMC 3, the Orion Nebula Cluster (ONC – also known as M 42), and an abundance of well-known low mass star forming cores, HH objects and bipolar outflows spread throughout the Lynds dark cloud L 1641 (HH 1/2, HH 33/40, HH 34, HH 38/43, etc.).

Our goals with these observations were to: (1) extend the maps of Stanke et al. (2002; hereafter Sta02) to give more complete coverage of Orion A, to search for new H_2 flows, and to better trace the true extent of known H_2 flows by searching for emission off the main molecular ridge; (2) provide a second epoch for proper motion studies, and (3) compare the observations with extensive (sub)millimetre and mid-IR Spitzer observations, so that H_2 jets and outflows could be associated with molecular cores and/or embedded protostars, the latter being identified from mid-IR photometry. We utilise the 850 μm SCUBA data published by Nutter & Ward-Thompson (2007), the more extensive 1200 μm MAMBO observations of Stanke et al. (in prep.), and the recent Spitzer observations of Megeath et al. (in prep.).

This paper is structured as follows: in Sect.3 we briefly discuss wide-field images of regions of interest spread throughout Orion A and give statistical information pertaining to the overall population of outflows. In Tables 2 and 3 we list the H_2 flows catalogued by Sta02 and the newly identified H_2 flows from this paper, respectively: in both tables we list the likely outflow source (if known), the dense cores that coincide with the source, and any HH objects that are associated with the flow. In Sect.4. we discuss the region as a whole, drawing statistical information from the sample of flows and associated sources. In Appendix A we briefly discuss the full sample of molecular H_2 outflows, presenting continuum-subtracted H_2 2.122 μm images of the newly-observed flows. In Appendix B we discuss our proper motion measurements for outflows observed here and in the earlier work of Sta02.

2. Observations

2.1. Near-IR imaging

Broad-band J, H, K and narrow-band H_2 2.122 μm images of a $1.5^\circ \times 1.5^\circ$ field centred on M 42/M 43 were obtained during instrument commissioning on 24 November 2004 (filter characteristics are described in Hewett et al. 2006). Broad-band K and narrow-band H_2 images of a ~ 8 square degree field were later secured during Director’s Discretionary Time (DDT), on 15-16 December 2005. K and H_2 images of a single 0.75 square degree segment centred on the Orion nebula were also obtained during Service observing time on 12 February 2007. The commissioning data have only been used to construct the colour images in Fig. 2; the later observations, which were secured under slightly better observing conditions, and when the instrument was better characterised, have been used for all other figures and analysis. The service data have been used to fill in a gap in the DDT data, where bright stars and saturation affects produced poor results in the processing.

The near-IR wide-field camera WFCAM (Casali et al. 2007) at UKIRT was used on each occasion. WFCAM houses four Rockwell Hawaii-II (HgCdTe 2048x2048) arrays spaced by 94% in the focal plane. The pixel scale measures 0.40”. To observe a contiguous square field on the sky covering 0.75 square degrees – a WFCAM “tile” – observations at four positions are required. At each position, to correct for bad pixels and array artifacts, a five-point jitter pattern was executed (with offsets of 3.2” or 6.4”); to fully sample the seeing, at each jitter position a 2×2 micro-stepped pattern was also used, with the array shifted by odd-integer multiples of half a pixel. 20 frames were thus obtained at each of the four positions in the tile. Eleven tiles in total were observed covering over 8 square degrees, through both broad-band K and narrow-band H_2 1-0S(1) filters. Exposure times of 5 sec \times 2-coadds and 20 sec \times 2-coadds were used with the K and H_2 filters, respectively. With the jitter pattern and micro-stepping the total on-source/per-pixel integration time in K was therefore 200 sec; in H_2 the total exposure time was 800 sec.

The DDT data were reduced by the Cambridge Astronomical Survey Unit (CASU), which is responsible for data processing prior to archiving and distribution by

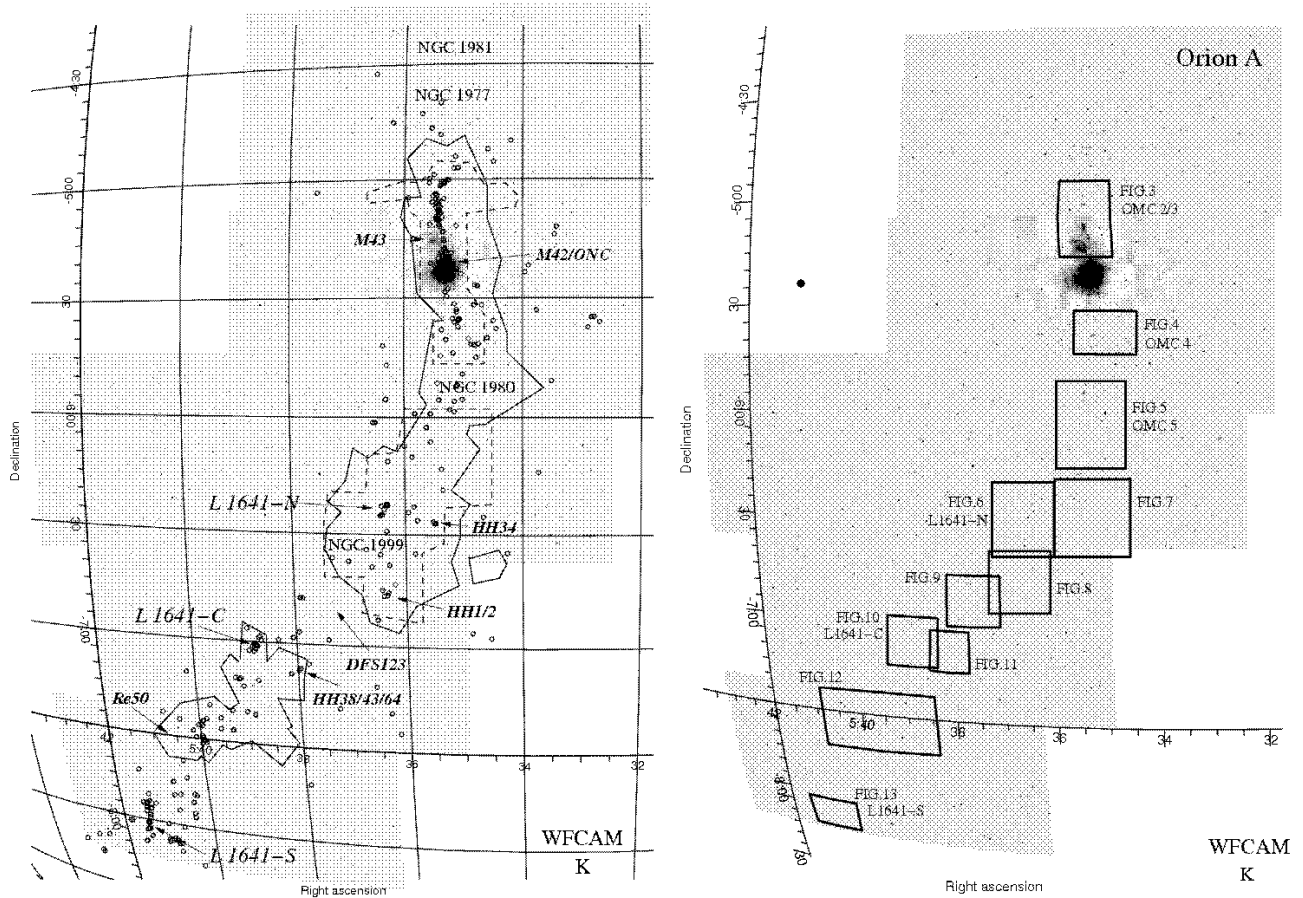


Fig. 1. Our near-IR K-band mosaic of Orion A. In the left-hand panel, the positions of candidate protostars identified from Spitzer photometry are marked with circles; the areas outlined with full lines have been mapped at $1200\mu\text{m}$ (Stanke et al., in prep.); the areas marked with dashed lines have been mapped at $850\mu\text{m}$ (Nutter & Ward-Thompson 2007). In the right-hand panel the regions shown in detail in Figs. 3 to 13 are indicated with boxes.

the Wide Field Astronomy Unit (WFAU). However, the processing of frames that included the bright Orion Nebula and Trapezium cluster gave images with severe background structure, probably related to the adopted method for sky-subtraction. Our service observations of this central region were therefore reduced using the ORAC-DR pipeline at the telescope (Cavanagh et al. 2003), which performs flat-fielding using twilight flats, but does not subtract a sky frame. The CASU reduction steps are described in detail by Dye et al. (2006). Residual sky/background structure was later removed by fitting a coarse surface to each image (as described by Davis et al. 2007). For both the CASU and Service data, astrometric and photometric calibrations were achieved using 2MASS (Dye et al. 2006; Hewett et al. 2006); the calibrated images were subsequently used to construct the large-scale mosaics presented in this paper.

In our K-band images we reach a limiting magnitude of ~ 18.3 in the less-nebulous regions; our sensitivity to point sources in the very bright Orion nebula regions is 2–3 magnitudes worse. In the H_2 images of L 1641, outflow features with a surface brightness of $\sim 7 \times 10^{-19} \text{ W m}^{-2} \text{ arcsec}^{-2}$ are detected

at $3\text{--}5\sigma$ above the surrounding background. The H_2 sensitivity in the ONC region is again lower because of the variable, diffuse nebulosity.

An overview of the region observed with WFCAM is given in Fig. 1; colour images of the spectacular OMC 1/2/3 regions are presented in Fig. 2; large-scale H_2 1-0S(1) mosaics of regions of interest throughout Orion A are presented in Figs. 3–13. Continuum-subtracted images of the newly-identified H_2 flows are available in Appendix A. In all of these figures axes are labelled in 2000.0 coordinates.

2.2. Proper motion measurements

Using the newly-acquired WFCAM images and the H_2 mosaics of Sta02, which were obtained between December 1996 and May 1998 with the 3.6-m telescope at the Calar Alto Observatory, Spain, we have measured tangential velocities for emission-line features in a number of flows. We focus on regions where multiple flows are observed, particularly where the association between outflows and embedded protostars is

Colour high-def picture available from <http://www.jach.hawaii.edu/~cdavis/>
Or see JPEG figure davis-fg2.jpg with this astro-ph submission.

Fig. 2. Left: colour image of OMC 1/2/3 composed of broad-band J, K and narrow-band H₂ 2.122 μm observations. The data have been stretched logarithmically. Right: colour J, H and narrow-band H₂ 2.122 μm composite of the region between Haro 5a/6a and M 43 (OMC 2/3). The data have again been stretched logarithmically. H₂ flows are labelled with “SMZ” or “DFS” numbers; outflow sources are labelled with “IRS” numbers. The dashed box in the left-hand image marks the area covered by the right-hand image.

ambiguous. A complete list of proper motions (PMs) is given in Appendix B, where the technique is described in detail.

2.3. Mid-IR observations

The Spitzer Space Telescope observations discussed in this paper were obtained with the IRAC and MIPS cameras (Fazio et al. 2004; Rieke et al. 2004). A full description of the data analysis and young stellar object identification will be presented in Megeath et al. (in prep); we provide here a brief summary.

Images in IRAC bands 1, 2, 3 and 4 (at 3.6, 4.5, 5.8 and 8.0 μm) and MIPS band 1 (at 24 μm) were used to compile a list of more than 300 candidate protostars between declinations -4.6° and -9.0° . The protostars were selected from their [3.6]-[4.5] and [4.5]-[24] colours (Megeath et al. 2009), although note that the majority of the sources would also be classified as flat spectrum, Class 0 and Class I protostars on the basis of their Spectral Energy Distributions (SEDs). To minimize contamination from extragalactic sources we rejected all sources with protostellar colours but 24 μm magnitudes fainter than 7. About 20% of the protostars were not detected at 24 μm and were therefore identified through their [4.5]-[5.8] colour using the approach of Gutermuth et al. (2008); most of these sources

are found in the Orion nebula where the 24 μm data were saturated.

There is a small amount of contamination from extragalactic sources, particularly AGN; we estimate this contamination to be 0.7 sources per sq. degree. In addition, there may also be some contamination from embedded Class II sources and potentially from edge-on young stars with flared disks. Estimates of the degree of contamination await the analysis of recent Spitzer 5-40 μm spectroscopy of the sample. In addition to the protostars, a further ~ 2000 disk excess sources were identified in the Spitzer data.

The sample of protostars is not complete: we expect that many protostars are hidden in the bright nebulosity toward the Orion nebula, and that several very bright protostars were omitted because of strongly saturation in the 24 μm data.

To characterize the SED of each protostar and disk excess source, a spectral index was obtained by fitting a single power-law to the 3.6, 4.5, 5.8, 8 and 24 μm photometry. For sources without 24 μm detections, the spectral index was calculated from only the IRAC photometry. The resulting 3.6-24 μm spectral-index, $\alpha = d\log(\lambda F(\lambda))/d\log\lambda$, ranges from -0.5 to 3.0 for the protostars. Although the spectral index is useful as an indicator of evolution, the index does depend on the density, the rotation rate, and the inclination of the protostellar envelope (Whitney et al. 2003,2004). Consequently, one should not

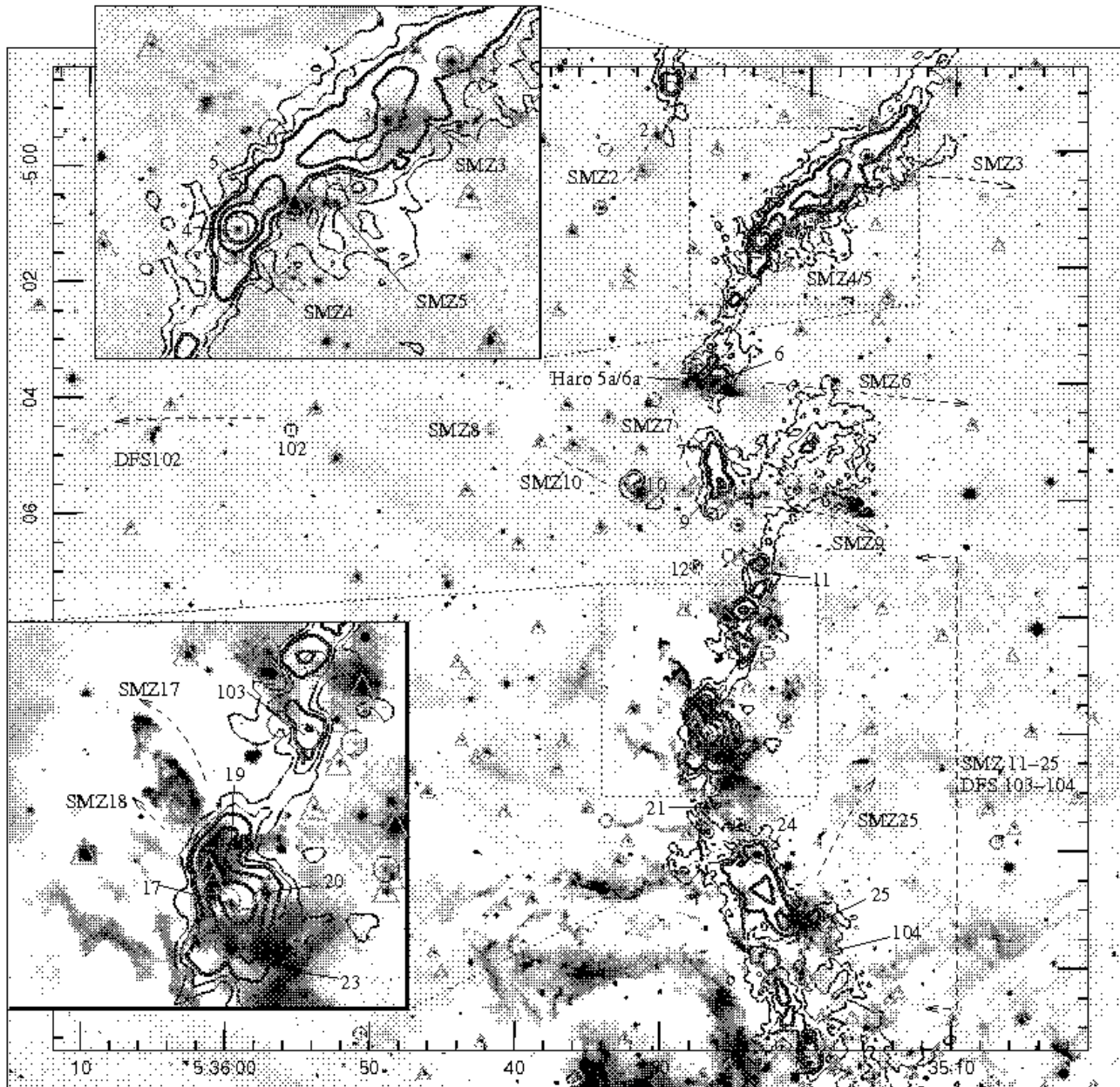


Fig. 3. Narrow-band H_2 $2.122\ \mu\text{m}$ images of OMC 2/3, the region directly north of the ONC in Fig. 1 (inset figures are double the scale and displayed with a logarithmic stretch). Here and elsewhere in this paper Spitzer protostars and disk sources are marked with circles and triangles, respectively. MAMBO $1200\ \mu\text{m}$ contours are over-plotted; levels measure 5σ , 7.5σ , 10σ , 20σ , 40σ , 80σ , etc., ($1\sigma \sim 20\ \text{mJy/beam}$ in central regions of the map where there is no emission). H_2 flows are labelled and marked with dashed arrows (see also Sta02).

expect a fool-proof relationship between α and the age of the protostar. A histogram showing the distribution of α for the protostars in Orion peaks at around 0 and gradually declines with increasing α . In contrast, the disk excess sources have spectral indices in the range $-2.5 < \alpha < 0.0$; a histogram of α values for these objects peaks at around -0.8, consistent with a large population of Class II objects. We note that the spectral indices of the disk excess sources can be affected by extinction. Hence, the distribution of their α values overlaps the distribution of α for the protostars (note that there is not a discontinuity in the distribution of α between the disk excess and protostars). This

may reflect a continuous transition between protostars and disk excess sources, as the infalling envelope is dissipated and the inner star/disk system is revealed.

2.4. (Sub)millimetre observations

In many of the subsequent figures we also overlay contours of dust continuum emission at $1200\ \mu\text{m}$. These data were obtained with the IRAM 30-m telescope at Pico Veleta, Spain, with the 37 and 117-pixel Max Planck Millimeter Bolometer (MAMBO) arrays (Kreysa et al. 1999). The data were ac-

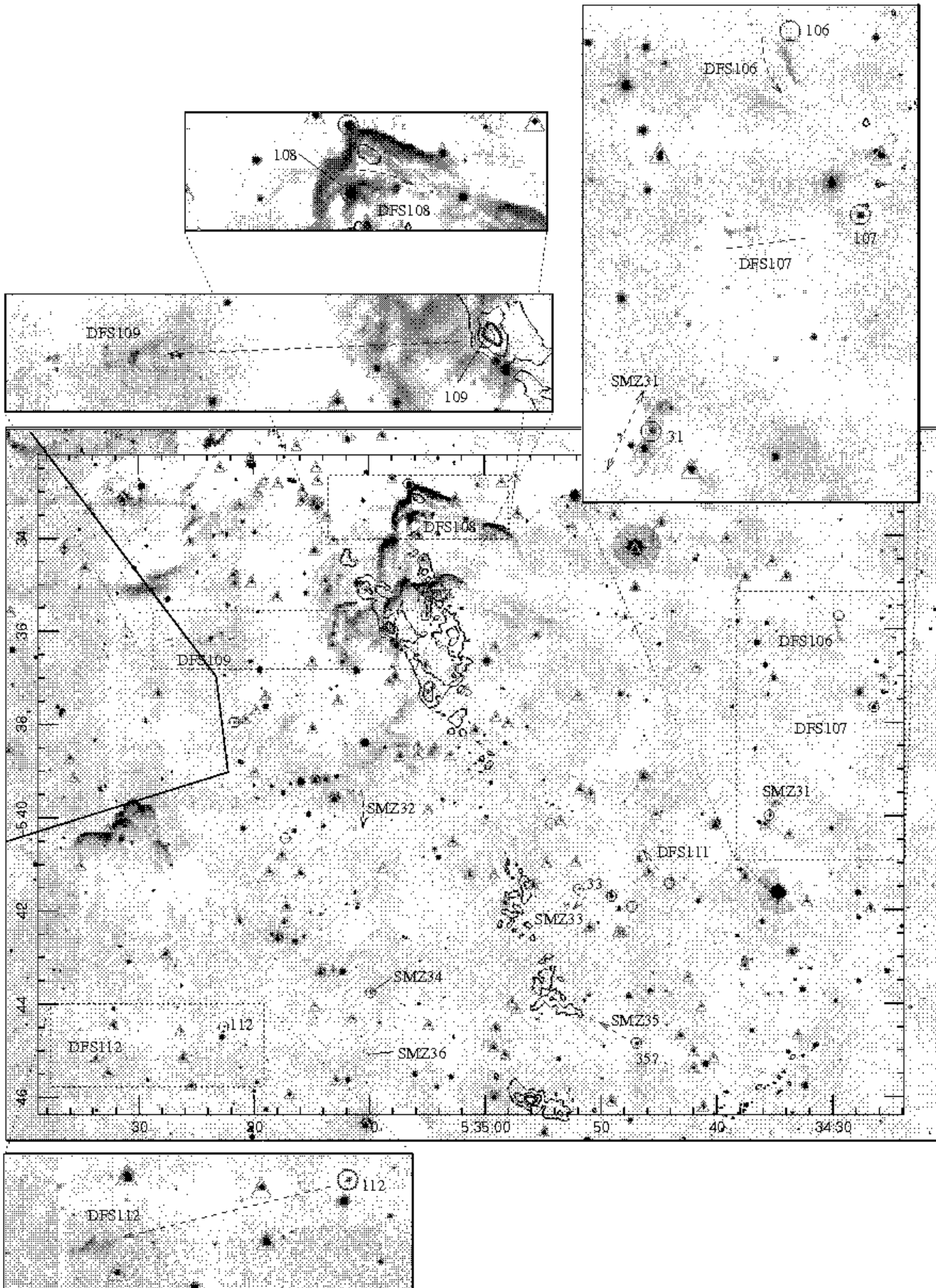


Fig. 4. Narrow-band H_2 $2.122\mu m$ images of the region $\sim 20'$ south of the ONC (Johnstone & Bally (2006) refer to this region as OMC 4). Inset figures are again double the scale and displayed with a logarithmic stretch. The full line on the left marks the edge of the MAMBO map. DFS 105, DFS 110 and DFS 114 lie to the west of the region shown above. Contours and symbols are as in Fig. 3.

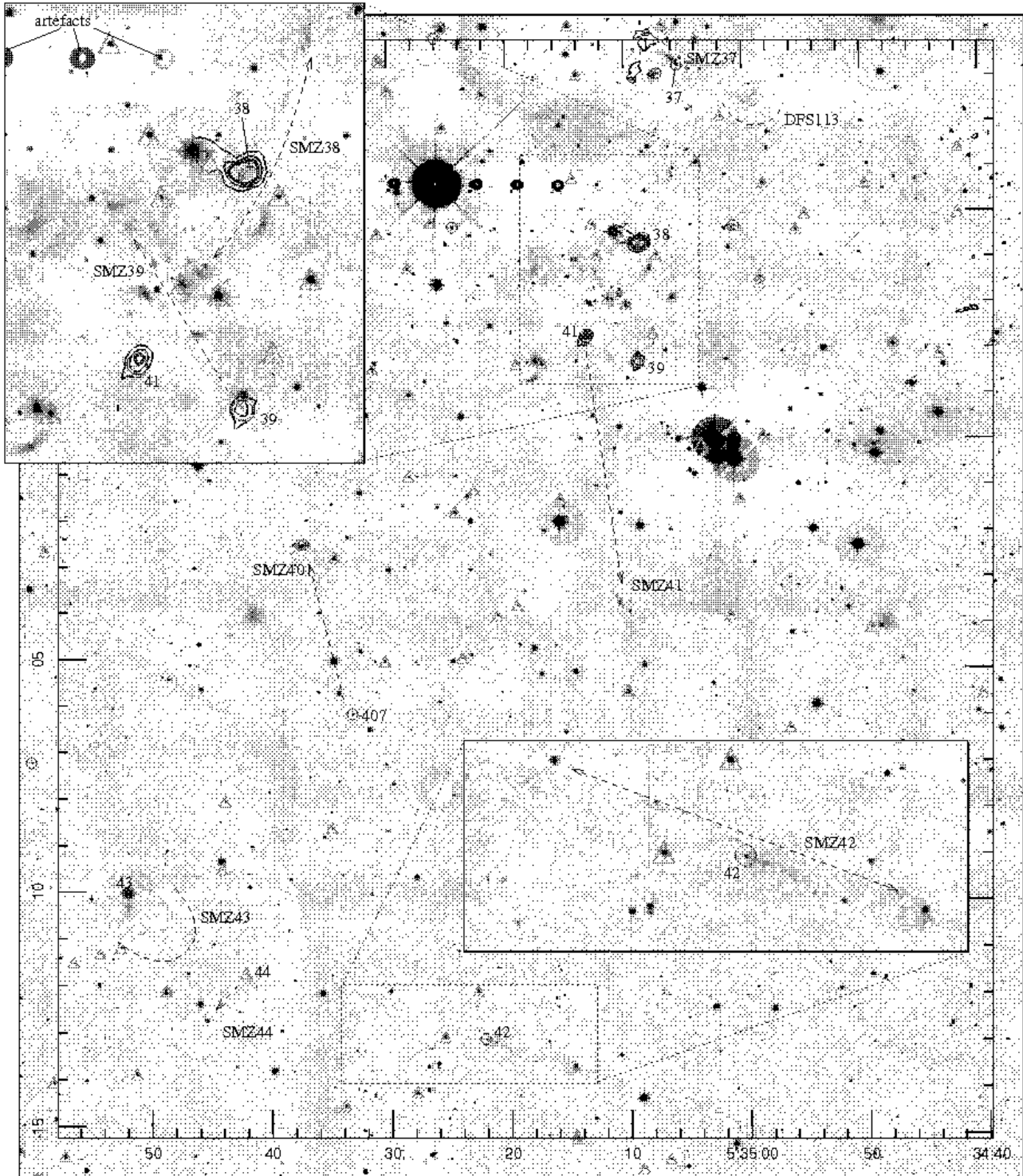


Fig. 5. Narrow-band H_2 $2.122\mu\text{m}$ images of the region around NGC 1980 – OMC 5 in Johnstone & Bally (2006) – about $45'$ south of the ONC (see Fig. 1). Inset figures are again double the scale and displayed with a logarithmic stretch. Contours and symbols are as in Fig. 3.

quired over several observing runs between 1999 and 2002, and reduced using the in-house reduction package “MOPSI”. Standard reduction steps were employed; baseline-fitting, despiking, correction for atmospheric extinction and flux calibration using planetary observations. At IRAM the MAMBO Half Power Beam Width (HPBW) measures $11''$.

A preliminary catalogue of ~ 500 MAMBO cores was obtained from visual inspection of the map and 2-dimensional Gaussian fitting of features. From this list we identify cores that coincide with an H_2 outflow source and list the core parameters in Tables 2 and 3. The MAMBO dataset will be analysed in detail in a future paper (Stanke et al., in prep.).

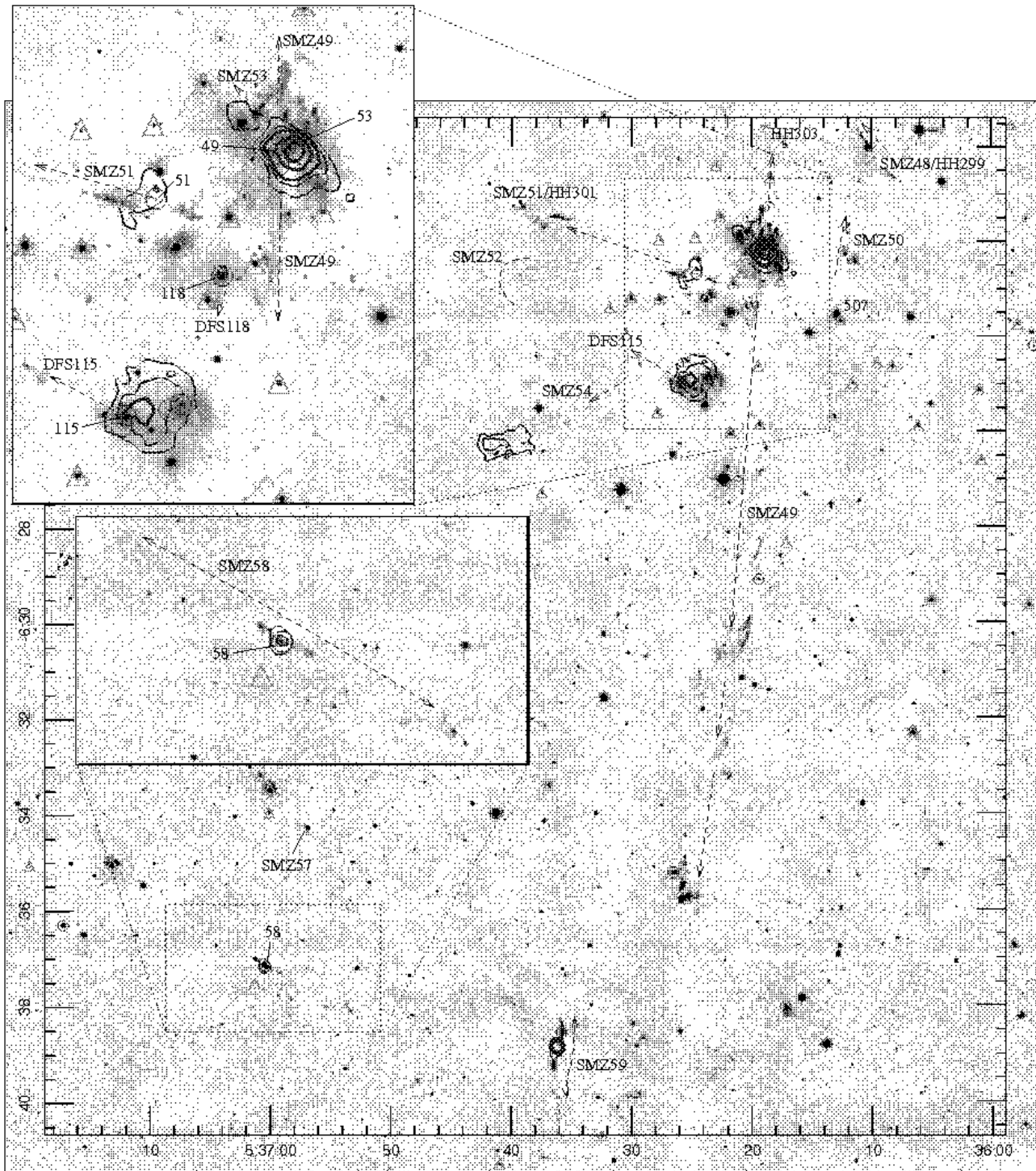


Fig. 6. Narrow-band H_2 2.122 μm images of L 1641-N (labelled in Fig. 1). Both insets are displayed at twice the scale and with a logarithmic stretch. Contours and symbols are as in Fig. 3.

3. Results

3.1. Overview

In Fig. 1 we present a mosaic of the complete K-band dataset. We indicate on this figure the extent of the 850 μm and 1200 μm maps, and mark the positions of ~ 300 protostars.

Colour images of the bright, nebulous regions around the ONC/M 42, the M 43 HII region, and the complex star form-

ing environment around Haro 5a/6a are shown in Fig. 2. These allow the reader to better distinguish H_2 -emitting jets and outflows from filaments of bright nebosity. Near-IR observations of the region around BN/KL, including the spectacular Orion Bullets, the Orion Bar, BN and the Trapezium cluster, have been discussed in many other papers (e.g. Usuda et al. 1996; Schild, Miller & Tennyson 1997; Lee & Burton 2000; Bally et al. 2000; Carpenter et al. 2001; Slesnick et al. 2004;

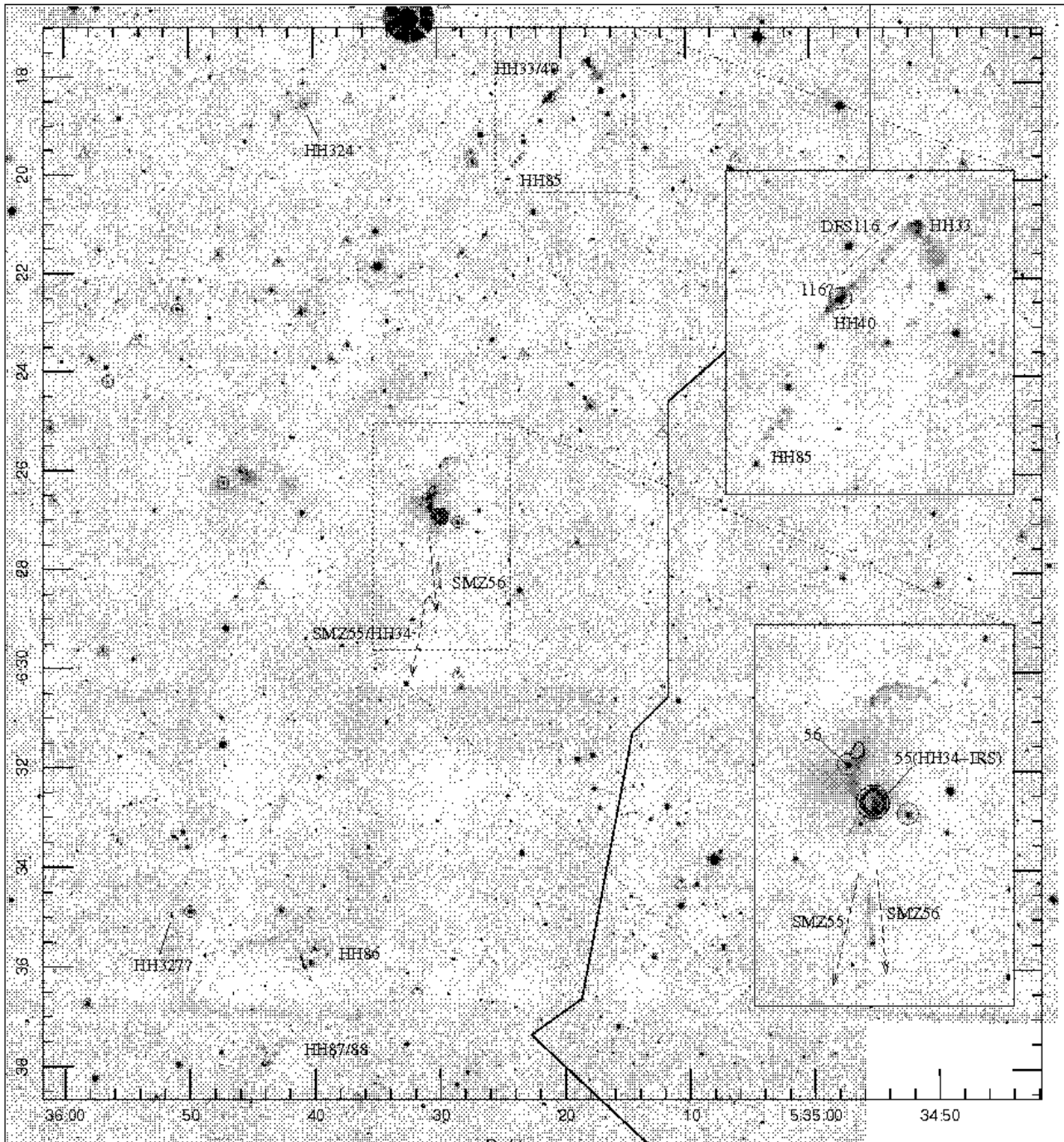


Fig. 7. Narrow-band H₂ 2.122 μm images of the region around HH 33/40 and HH 34 (roughly 0.5° west of L 1641-N – see Fig. 1). The zig-zag line through the centre of the image marks the western border of the MAMBO map. Both insets are again displayed at twice the scale and with a logarithmic stretch. Contours and symbols are as in Fig. 3.

Kassis et al. 2006; Simpson et al. 2006; Tamura et al. 2006). In this paper we therefore focus on the area to the north of the ONC, the OMC 2/3 region, and the extensive L 1641 low-mass star forming region to the south.

In Figs. 3-13 we present segments of the full H₂ mosaic, indicating with dashed lines the locations of H₂ jets and outflows (the data in these figures have been binned over 4×4 pixels, to a pixel scale of 0.8", to enhance the fainter features). Many of the outflows imaged here have already been catalogued by Sta02

(H₂ images of OMC 2/3 are also presented by Yu et al. 1997 and Yu et al. 2000). With the newly-identified H₂ flows, we therefore continue the numbering scheme of Sta02, although new flows (often found beyond the bounds of the Sta02 data) are numbered above 100. The Sta02 objects and the new H₂ outflows are prefixed with SMZ and DFS, respectively. Note that entire H₂ flows, rather than individual H₂ features or small groups of knots, are given a single number. For example, HH 1 and HH 2, which are relatively discrete objects, are here (and in

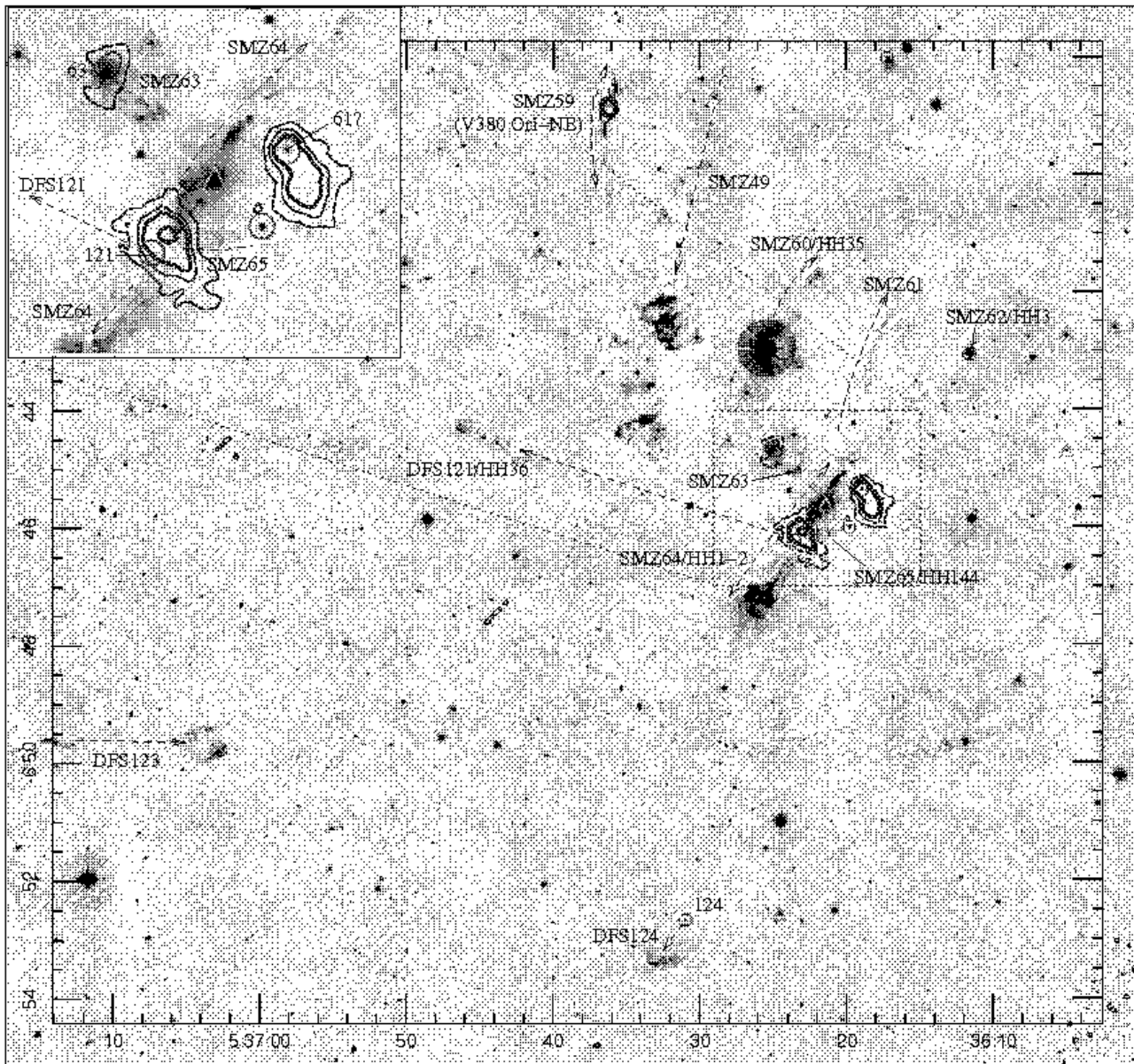


Fig. 8. Narrow-band H_2 2.122 μm images of the region around HH 1/2 in NGC 1999 (roughly 0.5° south of L 1641-N – see Fig. 1). The inset of HH 1 is double-scale and displayed with a logarithmic stretch. Contours and symbols are as in Fig. 3.

Sta02) referred to as SMZ 64. All H_2 flows are listed in Tables 2 and 3; continuum-subtracted H_2 images of the new DFS flows are given in Appendix A, along with a brief description of each outflow.

In Figs. 3-13 we also mark the positions of the protostars and (more numerous) disk excess sources identified from the Spitzer data; candidate outflow sources, when identified, are numbered using the same value as is given to the H_2 outflow itself (so for example DFS 101 is driven by IRS 101). Outflow sources are listed in Tables 2 and 3, together with any coincident molecular cores seen at $850 \mu\text{m}$ or $1200 \mu\text{m}$. $850 \mu\text{m}$ cores are taken from Nutter & Ward-Thompson (2007); the table of $1200 \mu\text{m}$ cores has yet to be published (Stanke et al., in prep.), so here we again use the outflow number, together with MMS (for MilliMetre Source), to identify each core.

The association of jets with young stars and/or (sub)millimetre continuum peaks is largely based on morphology and/or alignment. However, in some of the more complex regions we use the PM measurements in Appendix B to help isolate the location of the outflow source; in most cases the direction of propagation of the shock features are as one might expect, based on their morphology and the location of candidate outflow sources.

3.2. Outflow activity in Orion A

OMC 2/3 (Figs. 2 and 3), the region to the north of the ONC, is described in considerable detail by Yu et al. (2000). HH objects are identified by Reipurth, Bally & Devine (1997) and Bally & Devine (2001). High-resolution CO outflow maps are presented by Williams et al. (2003). The distribution of dense

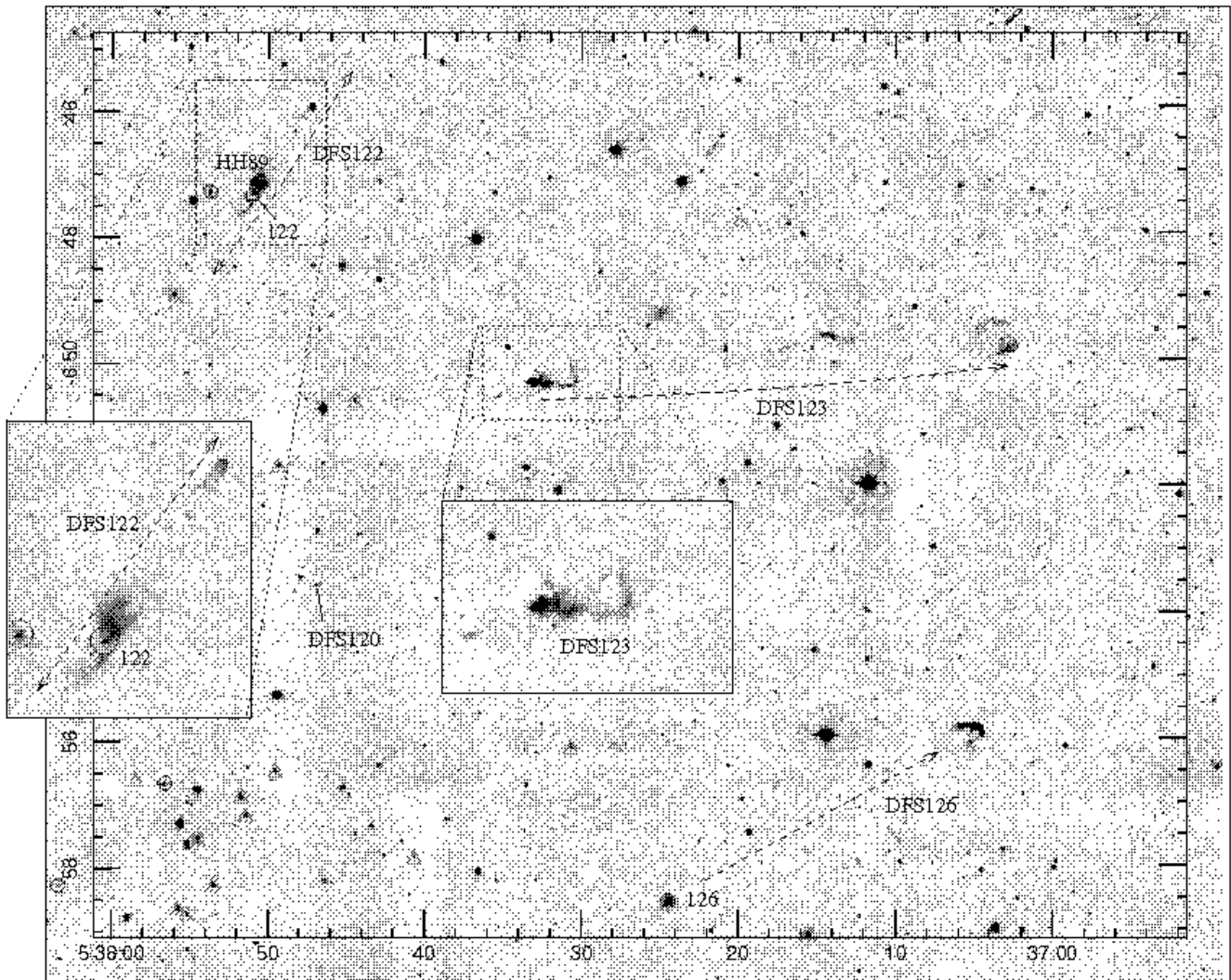


Fig. 9. Narrow-band H_2 2.122 μm images of the region $\sim 0.5^\circ$ east of HH 1/2 in NGC 1999 (see Fig. 1). Both insets are displayed at double-scale and with a logarithmic stretch. Note that the MAMBO 1200 μm (and SCUBA 850 μm) maps do not cover this region. Symbols are as in Fig. 3.

molecular gas throughout OMC 1/2/3 has been mapped at 450 μm and 850 μm by Johnstone & Bally (1999); Chini et al. (1997) present 1300 μm observations of OMC 2/3. A comprehensive review is also given by Peterson & Megeath (2008).

The vast majority of protostars in Fig. 3 are located within 11'' of a MAMBO core and/or 14'' of a SCUBA core (these radii being equivalent to the HPBW of these (sub)millimetre data). The association of bright H_2 jets with Spitzer protostars and cold molecular cores attests to the youth of the outflows in this region. Most of the protostars are located along the chain of cores that runs through the centre of OMC 2/3 (the disk excess sources are more widely distributed); similarly, most of the H_2 outflows seem to be driven by sources close to this central axis. The most distinctive H_2 flows, SMZ 3, SMZ 5, SMZ 6 and SMZ 9 are also orientated perpendicular to the north-south axis of cores.

From Sta02 there are 22 H_2 flows spread across the region shown in Fig. 3 (we regard SMZ 11 and SMZ 13 as a single flow; likewise SMZ 14/16 and SMZ 21/22). We identify four

new H_2 flows north of the ONC, DFS 101-104. Candidate outflow sources are found for 24 of the 26 H_2 flows. Only two have negative spectral indices; the rest are either “flat spectrum” or reddened protostars. Two of the 25 Spitzer outflow sources were not observed with MAMBO; of the remaining 23, 18 are associated with 1200 μm (MMS) cores.

In Figs. 4 and 5 we show large-scale H_2 images of two regions south of the ONC, adjacent to NGC 1980 in the overview plot in Fig. 1. Johnstone & Bally (2006) refer to these regions as OMC 4 and OMC 5, respectively. In and around these two areas Sta02 identify at least 18 possible H_2 flows (SMZ 29–SMZ 46; between declination $-5^\circ 20'$ and $-6^\circ 15'$); we add a further ten H_2 flows to this tally (DFS 105–114; note that DFS 105, DFS 110 and DFS 114 are beyond the edges of Fig. 4). Moreover, PMs have been measured for many of the flows in this area.

We identify candidate outflow sources for 25 of the 28 outflows in the OMC 4 and 5 regions, although unlike OMC 2/3, many of these sources are not associated with dust cores. (Note

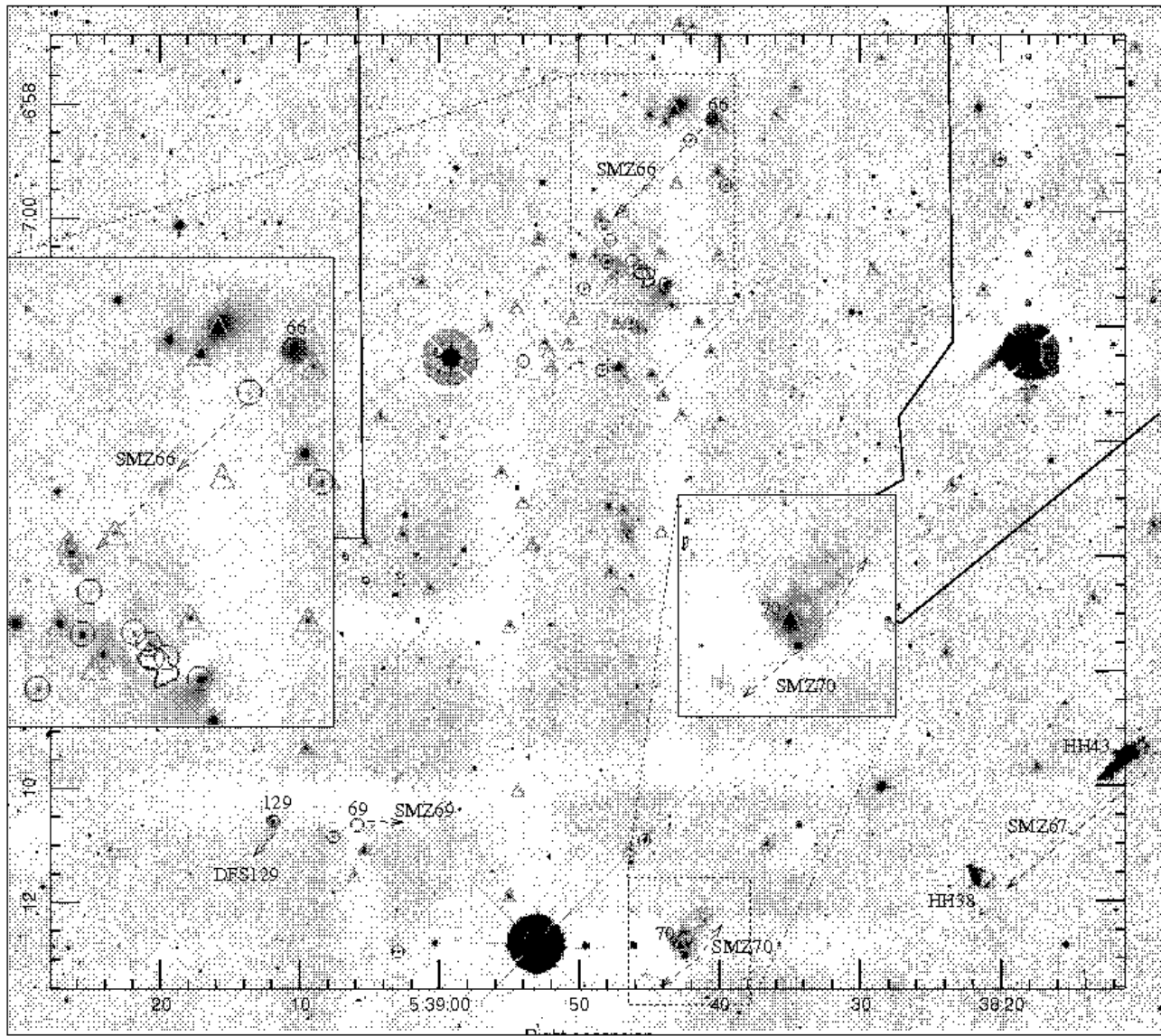


Fig. 10. Narrow-band H_2 $2.122\mu m$ images of L 1641-C (labelled in Fig. 1). Both insets are displayed with a logarithmic scale and at twice the scale of the main figure. The northeast and northwest edges of the MAMBO map are marked with full lines. Contours and symbols are as in Fig. 3.

that Johnstone & Bally (2006) also compare H_2 images with dust continuum maps in this region, using the images of Sta02 and their SCUBA observations, respectively.) All of the SMZ jets were observed with MAMBO, as were seven of the 10 DFS flows. However, only 14 of the 25 observed H_2 outflow sources are associated with $1200\mu m$ cores. There are clearly considerable differences between the star forming regions north of the ONC (OMC 2/3), and those directly south (OMC 4/5).

As we move further south (through L 1641-N towards L 1641-C, see Fig. 1) fewer protostars are identified in the Spitzer analysis. Even so, many sources are clearly driving H_2 flows: in many regions (e.g. around L 1641-N, HH 34 and HH 1/2 in Figs. 6, 7 and 8) we note a clear association between Spitzer protostars, (sub)millimetre cores and H_2 outflows.

The infrared jets and outflows in the very busy region around L 1641-N (Fig.6) are described in detail by

Gålfalk & Olofsson (2007) and Stanke & Williams (2007). The former present Spitzer observations and PMs for knots close to L 1641-N itself; the latter show high-resolution CO maps that reveal a number of bipolar outflows centred on this cluster. The HH objects in the region are discussed by Reipurth, Devine & Bally (1998). Sta02 identify seven H_2 flows in and around L 1641-N (SMZ 48–SMZ 54); we label two additional flows, DFS 118 – which is associated with a bipolar CO outflow (Stanke & Williams 2007), and DFS 115 – which is associated with a small cluster of protostars $\sim 3'$ south of L 1641-N, known as Strom 11. Six of these nine H_2 flows have candidate Spitzer protostellar sources; all but one of these protostars is associated with $1200\mu m$ emission or a MAMBO core. In total there are 10 protostars within a $5'$ radius of L 1641-N; it seems likely that most, if not all of these sources could be associated with H_2 line emission features.

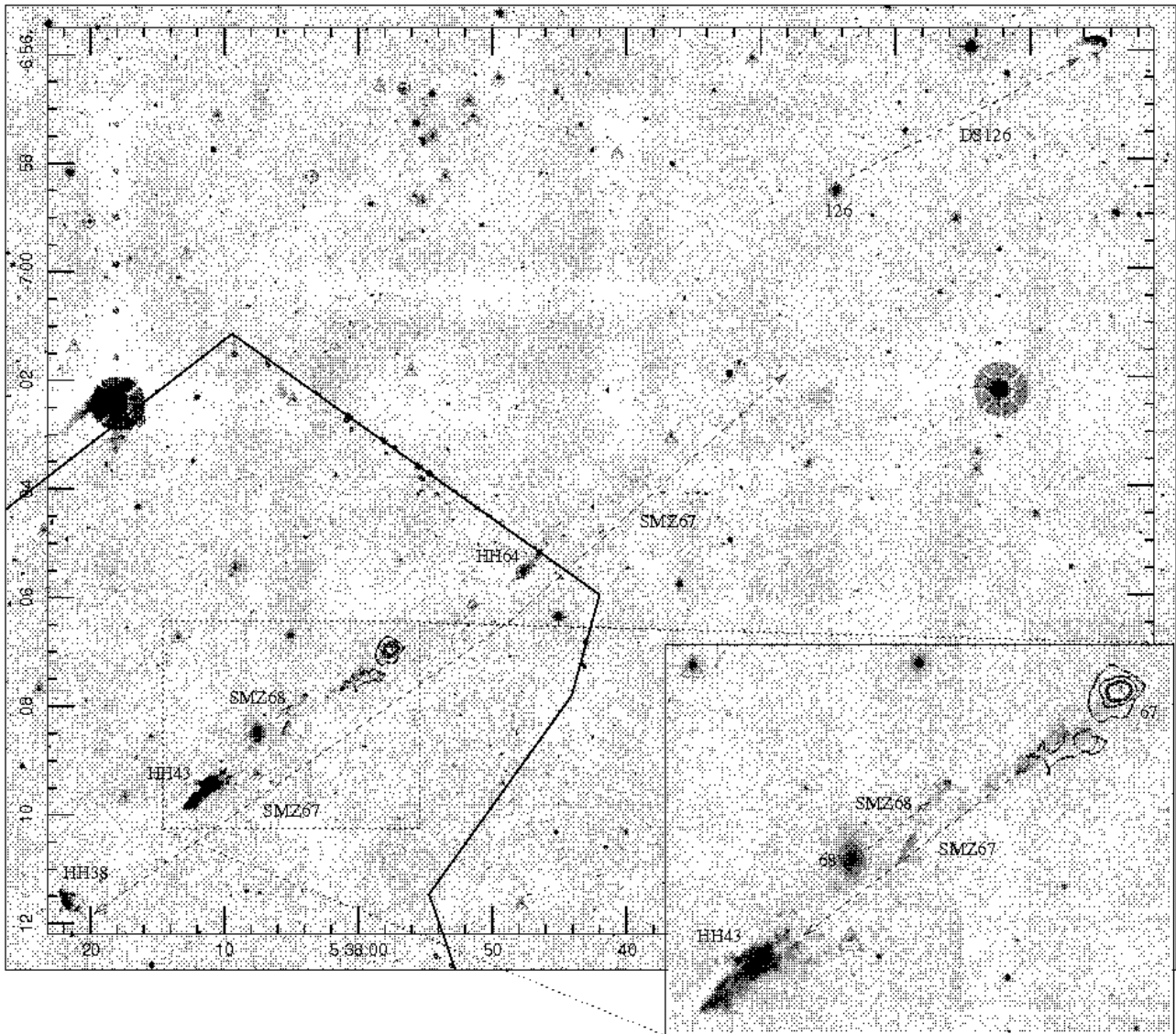


Fig. 11. Narrow-band H_2 $2.122\ \mu\text{m}$ images of the region $\sim 0.3^\circ$ west-southwest of the L 1641-C cluster that includes the extensive HH 38/43/64 bipolar outflow (see Fig. 1). HH 43 and its source are shown inset at double-scale with a log stretch. The northern and western edges of the MAMBO map are marked with a full line. Contours and symbols are as in Fig. 3.

The region to the west of L 1641-N, around HH 34, is shown in Fig. 7. The source of the well-known HH 34 jet, HH 34-IRS (IRS 55), is flagged as a protostar in the Spitzer data, along with two other sources, one of which (IRS 56) drives a second H_2 flow. North of HH 34, the well-known HH objects HH 33/40 have in recent years been considered to be part of a parsec-scale flow that includes HH 34 and HH 86/87/88 to the south (Devine et al. 1997; Eislöffel & Mundt 1997). However, in the Spitzer analysis a protostar (IRS 116) is found coincident with HH 40. The source is point-like in $24\ \mu\text{m}$ MIPS data so is probably not a misidentified H_2 features¹. IRS 116 is not associated with a dense

SCUBA or MAMBO core. Even so, it remains a viable candidate outflow source for HH 33/40.

Roughly $25'$ west of HH 34, HH 83/84 (Reipurth 1989) is also observed in H_2 emission. HH 83-IRS, the source of this well-known jet, is outside the bounds of the SCUBA and MAMBO observations, and the Spitzer IRAC $3.6\ \mu\text{m}$ and $5.8\ \mu\text{m}$ and MIPS $24\ \mu\text{m}$ maps, although a bright source is detected in the remaining IRAC bands with an infrared excess. HH 83-IRS's [4.5]-[8] color is more consistent with a disk excess source than a protostar.

The outflows in the vicinity of HH 1/2, shown here in Fig. 8, are well documented (see e.g. Davis, Eislöffel & Ray 1994; Hester, Stapelfeldt & Scowen 1998; Reipurth et al. 2000). Radial velocities and PMs – based on optical observations –

¹ H_2 features produce pure-rotational emission lines in each of the four Spitzer IRAC bands, though not in the MIPS $24\ \mu\text{m}$ band (e.g. Smith & Rosen 2005; Velusamy, Langer & Marsh 2007). Spectral indices measured from the IRAC bands alone can therefore mimic val-

ues expected for protostars (Davis et al. 2008), though a MIPS detection would then require bright, forbidden line emission from [FeII].

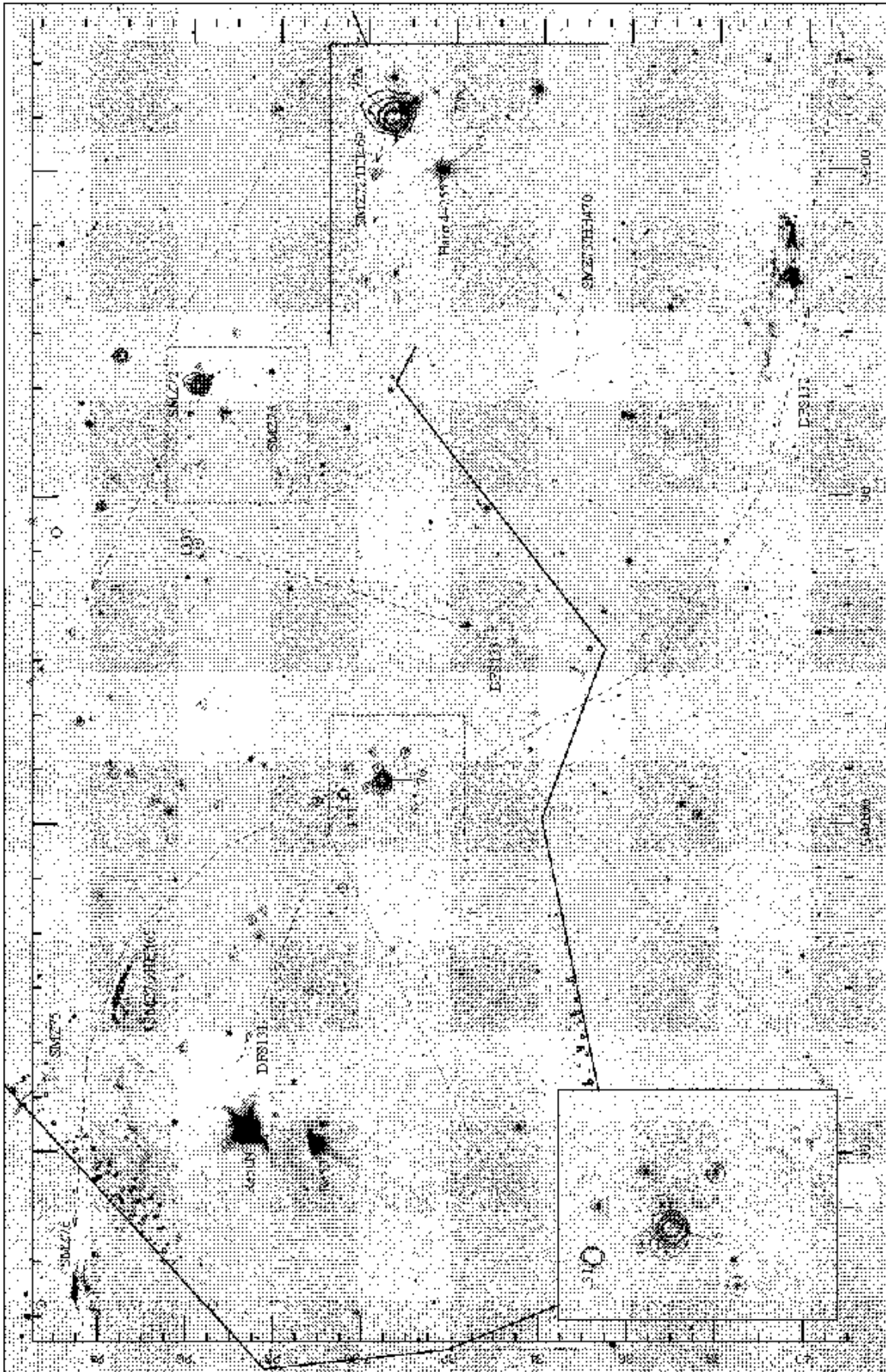


Fig. 12. Narrow-band H_2 2.122 μm images of the region around Re 50 and Haro 4-255, midway between L 1641-C and L 1641-S in Fig. 1. The figures inset show the regions around Haro 4-255 and the likely source of SMZ 76 (both displayed with a log stretch/double size). The southern edges of the MAMBO map are marked with a full line. Contours and symbols are as in Fig. 3.

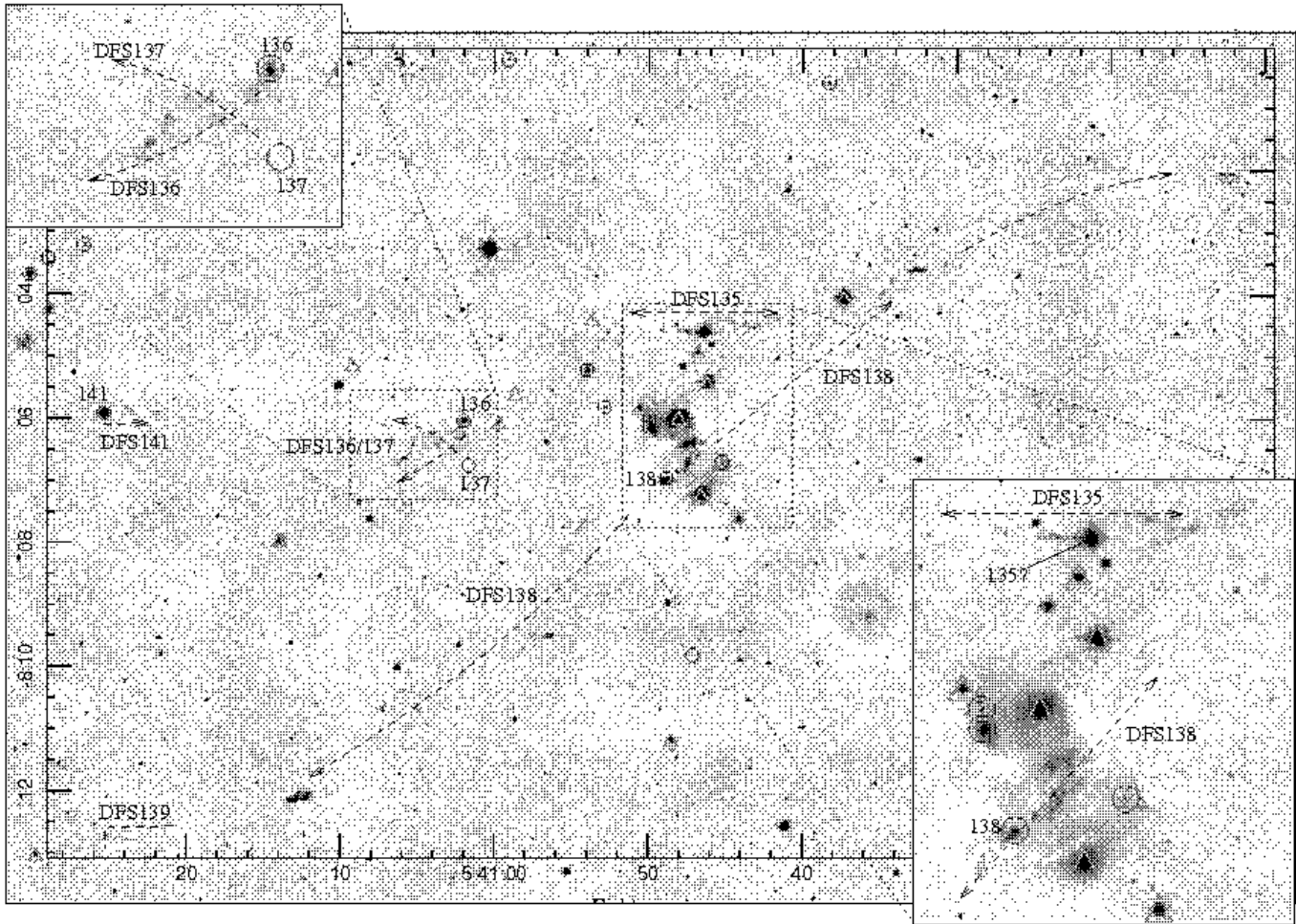


Fig. 13. Narrow-band H_2 $2.122\mu\text{m}$ images of L 1641-S, at the bottom of the overview mosaics in Fig. 1. No MAMBO (or SCUBA) observations are available for this region. The figures shown inset are displayed at twice the scale and with a log stretch. Symbols are as in Fig. 3.

have been reported in the literature for the central bright HH flows (Eisloffel, Mundt & Böhm 1994; Bally et al. 2002), so we have only measured PMs for the bright H_2 features 4'–5' northeast of HH 1/2. We find that these knots are moving southward, which confirms their proposed association with the large-scale SMZ 49 outflow. Around HH 1/2 itself, only four Spitzer protostars are identified (SMZ 62/HH 3 is probably a mis-identified H_2 knot). Three of the four protostars are associated with $1200\mu\text{m}$ cores; all four sources likely drive H_2 flows. The well-known VLA source of the HH 1/2 outflow is unresolved from neighbouring sources and therefore is not listed as an “IRS” source in Table 2.

By extending the maps to the southeast and southwest of the HH 1/2 region we discover six more H_2 flows, DFS 120 and DFS 122–DFS 126, four of which are shown in Fig. 9 (DFS 122 is associated with HH 89; Reipurth 1985). Three of the six have candidate protostellar sources (one was not observed with Spitzer). With a length of 1.1 pc, DFS 123 qualifies as a “parsec-scale” flow.

Roughly 30' to the southeast of HH 1/2, the Spitzer data recover the cluster of young stars collectively known as L 1641-C (Fig. 10). However, like Sta02 we identify only one clear-cut

flow in the region, SMZ 66. The cluster is associated with only faint $1200\mu\text{m}$ emission and so L 1641-C probably harbours a fairly evolved population. The absence of ambient material explains the lack of H_2 flows.

Fig. 11 shows the parsec-scale flow HH 38/43/64 (SMZ 67). The source of this outflow, and the neighbouring H_2 jet SMZ 68, are both retrieved from the Spitzer data. These protostars are also associated with molecular cores. If we include the DFS 126 bow-shock in the HH 38/43/64 outflow, then the total length of this system is 25' (3.2 pc).

The region midway between L 1641-C and L 1641-S (Fig. 12; see also Fig. 1 for reference) includes the well-known T Tauri star Haro 4-255 (Aspin & Reipurth 2000), its infrared neighbour Haro 4-255 FIR, and the spectacular arc of H_2 emission, SMZ 76, first noted by Stanke (2000). SMZ 74 (not shown here), SMZ 75 and SMZ 76 all have morphologies and PMs that imply motions away from the chain of young stars near the centre of Fig. 12, although precise associations are difficult to make. Stanke (2000) identified a millimetre peak southwest of SMZ 76 (which he labeled L 1641-S3 MMS1) as the location of the likely source of this object; we note that DFS 132 may be the counter-lobe of this remarkable outflow. The protostar/dust

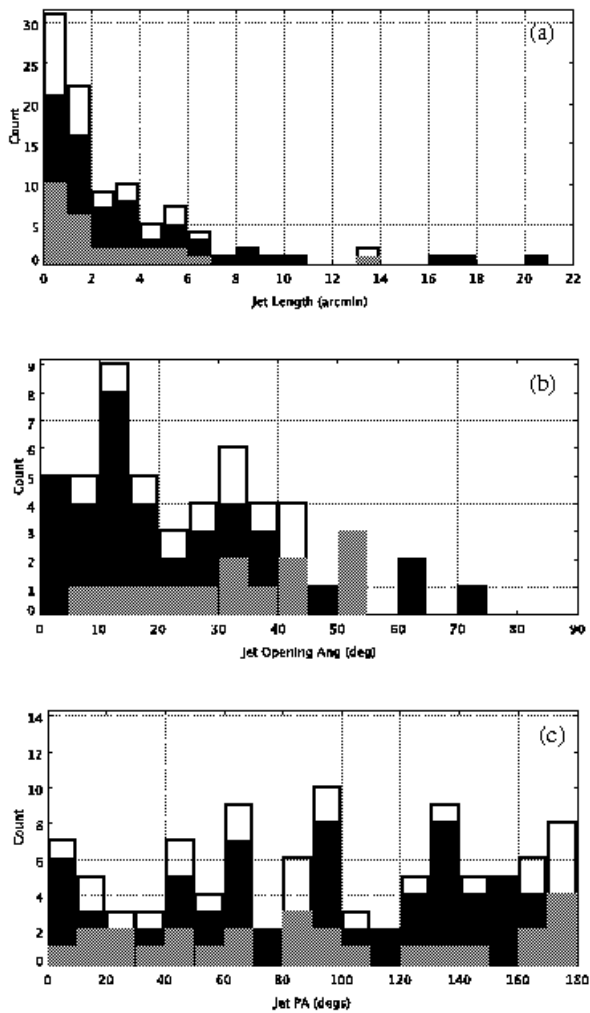


Fig. 14. Histograms showing (a) the distribution of jet lengths (in $1'$ bins), (b) jet opening angles (5° bins), and (c) jet position angles (10° bins), for all H_2 jets in Orion A (open columns), for H_2 flows north of the ONC (declination $> -5^\circ 30'$; grey filled columns) and for H_2 flows south of the ONC ($< -5^\circ 30'$; black filled columns).

core IRS 131/MMS 131 may also drive an H_2 flow (DFS 131), though there are perhaps a dozen Spitzer YSOs in this region with no obvious H_2 jet. Most have no associated dust core and are therefore, like the young stars in L 1641-C, probably too evolved.

Lastly, the region at the southern end of L 1641 is abundant with Spitzer-identified protostars and newly discovered H_2 flows. In Fig.13 we label six possible outflows, four of which have candidate sources (note that the MAMBO observations do not extend this far south in L 1641). DFS 138 is the most spectacular H_2 flow, comprising a bright, collimated, bipolar jet and sweeping bow shocks. The flow extends over $13.4'$ (1.8 pc) and is probably driven by the Spitzer protostar labelled IRS 138.

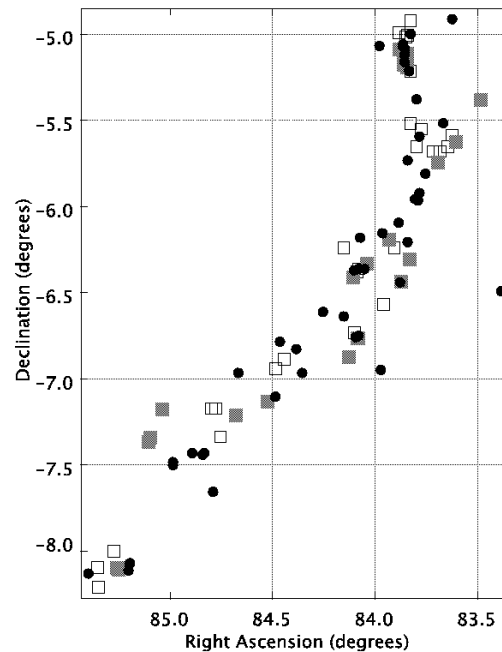


Fig. 15. A map showing the distribution of short ($L < 1'$; open squares), intermediate ($1' < L < 2'$; filled grey squares), and long ($L > 2'$; filled black circles) H_2 jets.

3.3. Outflow statistics

In Tables 2 and 3 we list 116 jets, of which 43 are newly identified. Of the 111 flows that were within the bounds of the Spitzer observations, 72 (62%) have catalogued Spitzer protostellar sources: a further 12 flows are tentatively associated with Spitzer sources (IRS source numbers marked with a question mark in Tables 2 and 3). Two well-defined flows, HH 1/2 and V380 Ori-NE, have established sources that were not flagged as young stars in the analysis of the Spitzer data (the former because it is too faint; the latter because it is too close to a neighbouring source); a third object, HH 83, was only observed in two of the four Spitzer IRAC bands. Closer examination of the mid-IR data shows that HH 1/2 and V380 Ori-NE are probably driven by protostars, and HH 83 by a disk excess source.

In total, 97 H_2 outflows (including all of the SMZ jets) were observed with MAMBO at $1200\mu\text{m}$. 53 (55%) are associated with MAMBO (MMS) cores *and* young Spitzer sources; a further four outflow sources are associated with extended $1200\mu\text{m}$ emission or are unresolved from brighter, nearby cores.

Of the 116 jets, 68 (59%) exceed an arcminute in length (at a distance of 450 pc, $1'$ is equivalent to 0.13 pc); 10 are parsec-scale jets, exceeding $7.6'$ (SMZ sources 6, 49, 55, 67, 76 and the newly-discovered DFS flows 117, 123, 132, 133 and 138). Throughout Orion A we measure a range of jet lengths (as traced in H_2); a histogram showing the distribution of lengths, uncorrected for inclination angle, shows that the number of flows with a given length decreases more-or-less exponentially (Fig. 14a). The same trend is seen if we just consider flows north of the ONC or flows south of the ONC: the map in Fig. 15

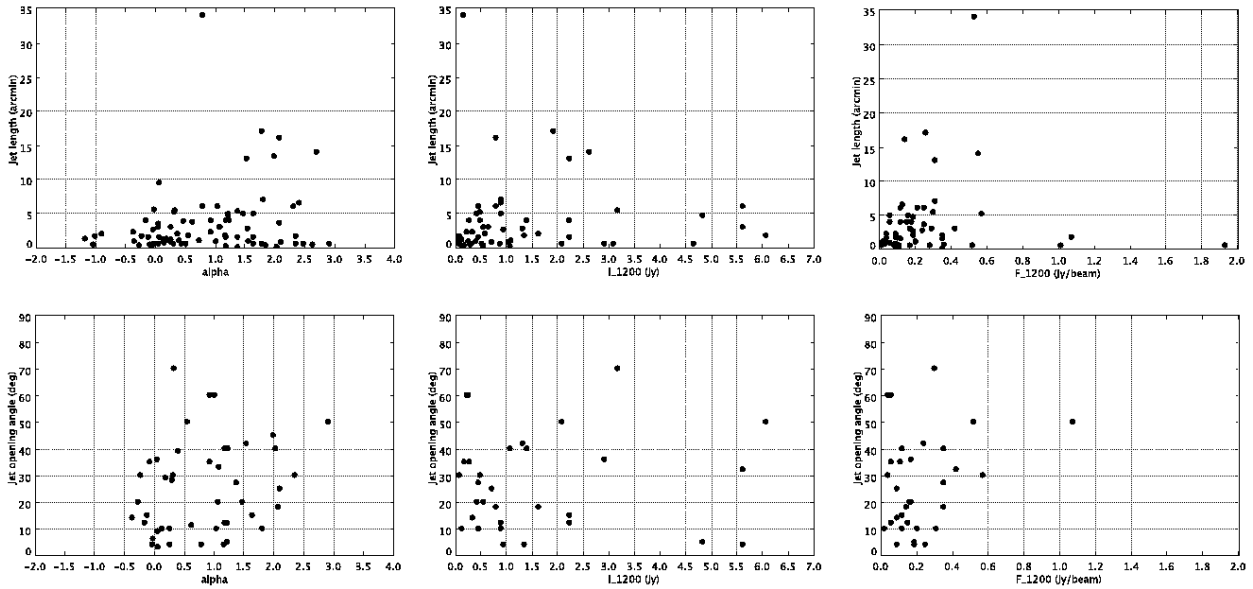


Fig. 16. Source spectral index, α , integrated $1200\mu\text{m}$ core flux, I_{1200} , and $1200\mu\text{m}$ flux density, F_{1200} , plotted against H_2 jet length and jet opening angle for all jets in Orion A with identified sources (Tables 2 and 3).

shows that the distribution of short ($L < 1'$), medium-length, and long ($L > 2'$) jets is more-or-less even across Orion A.

The jet lengths in Tables 2 and 3 are of course lower limits, since they are uncorrected for inclination to the line of sight. Also, as a jet or wind exits its molecular cloud, it will no longer entrain and shock-excite molecules and may not be visible in H_2 emission. The histograms in Fig. 14a are therefore biased towards shorter flow lengths. Even so, if all of the jets were of equal length and randomly inclined with respect to the line of sight, inclination alone would produce a histogram that increases towards longer jet lengths (peaking at an angle of $\pi/2$, neglecting any selection effects due to detectability as a function of angle). We can therefore be sure that the “ H_2 flows” in Orion are mostly short; macro-jets are a rare occurrence and, statistically at least, H_2 jet lengths do not appear to be dictated by the changing environment in Orion A.

We find no real correlation between H_2 jet length and indicators of the outflow source age, such as the spectral index, α (defined in Sect. 2.3), the integrated $1200\mu\text{m}$ flux of the core associated with each outflow source, I_{1200} , or the $1200\mu\text{m}$ surface brightness measured towards each outflow source, F_{1200} (Fig. 16 - note that F_{1200} is not always the flux density measured towards the core peak). Five of the six longest H_2 flows are associated with IRS sources with large spectral indices ($\alpha > 1.5$), though at the same time four of these five protostars seem to be associated with modest-sized cores ($I_{1200} < 1.5$ Jy; $F_{1200} < 0.6$ Jy) – the fifth protostar was not observed with MAMBO. The longest H_2 jet in Orion A, SMZ 49 ($L \sim 35'$), is almost certainly driven by a source in the compact L 1641-N cluster, which is associated with highly-reddened protostars and dense, massive molecular cores. However, identifying this remarkable jet’s progenitor and, in particular, resolving the associated core, is difficult.

There is some indication from millimetre observations of CO outflows that Class 0 sources produce more collimated flows than their Class I counterparts (Lee et al. 2002; Arce & Sargent 2006). This may be due to the destruction of the protostellar core by the outflow itself, as it entrains and plows away the ambient gas. Since H_2 emission traces the interaction of outflows with the surrounding molecular gas, one might expect to see some indication of this “flow broadening” in H_2 images of outflows from sources with lower values of α , or low values of I_{1200} . However, this does not seem to be the case: the flow opening angle, defined as a cone that encloses all H_2 emission line features, with an apex centred on the outflow source, appears to be unrelated to α , I_{1200} or F_{1200} (Fig. 16).

If we simply compare sources associated with a molecular core with sources undetected in $1200\mu\text{m}$ emission, we again find that both samples essentially have the same distributions of H_2 jet lengths and jet opening angles: for H_2 jet sources with cores the mean length is $3.9'$ (standard deviation = $5.6'$; range = $0.2'–34'$); for those without cores the mean length is $1.7'$ (std dev = $1.9'$; range = $0.1'–9.5'$). The former is skewed somewhat by the fact that four of the seven longest H_2 flows ($L > 10'$) are associated with IRS sources that do coincide with $1200\mu\text{m}$ cores (the other three long flows were not observed at $1200\mu\text{m}$). The mean opening angles for H_2 jets with and without cores are 27.7° (std dev = 18° ; range = $4^\circ–70^\circ$) and 19.9° (std dev = 15° ; range = $3^\circ–50^\circ$), respectively.

The lack of a correlation between α and H_2 jet length, L , or opening angle, θ , may be a result of the fact that α varies with orientation as well as source “age” (e.g. Whitney et al. 2003). More evolved sources driving the longest jets are expected to have lower spectral indices. However, jets inclined towards the observer will appear shorter and will likewise have lower spectral indices. Poor resolution and source confusion may also explain the lack of a correlation between core parameters (I_{1200}

and F_{1200}) and L or θ . One should also note that H_2 is not always an ideal measure of flow parameters. As noted earlier, H_2 excitation only occurs when the flow impacts dense ambient material, and pre-existing H_2 features cool and fade very rapidly (within a few years). For a flow that exits a molecular cloud, H_2 emission features will not be observed, so the true jet length may be underestimated. Conversely, jet opening angles may be over-estimated: the wings of jet-driven bow shocks are often much wider than the underlying jet (SMZ 42 is a nice example of this in Orion), and changes in flow direction due to precession will, over time, increase the apparent opening angle.

Finally, the precise relationship between α and source age has not yet been established. Spectral typing of protostars is difficult because of extinction and veiling of photospheric absorption lines (Greene & Lada 2002; Doppmann et al. 2003; Beck 2007; Antonucci et al. 2008), so age estimates based on the fitting of theoretical mass tracks and isochrones, especially for the youngest sources, can be problematic (see e.g. Doppmann et al. 2005). Radio continuum observations may be a better way to quantify the youth of an outflow source.

3.4. Flow orientations

H_2 jet position angles on the sky should be well defined, provided the outflow source is correctly identified. H_2 surveys can therefore be used to test the standard paradigm that clouds collapse along field lines to form elongated, clumpy filaments from which chains of protostars are born (Mouschovias 1976; Larry et al. 2008), with the associated outflows aligned parallel with the local field, and perpendicular to the chains of cores (Banerjee & Pudritz 2006). The presence of magnetic fields in molecular clouds has been demonstrated, and the orientations of field lines with respect to chains of oblate cores have been measured in a number of star forming regions (e.g. Crutcher et al. 1999; Matthews et al. 2002; Houde et al. 2004; Vallée & Fiege 2006; Larry et al. 2008). In a few regions there is also some indication that outflows are preferentially orientated orthogonal to individual cores or chains of cores, and/or parallel with the local magnetic field (Strom et al. 1986; Heyer, Strom & Strom 1987; Ménard & Duchene 2004; Davis et al. 2007; Ananthapindika & Whitworth 2008).

The Orion A GMC comprises a large number of cores extended along a north-south “integral-shaped” filament that passes through the Orion nebula and extends southward, broadening out between L 1641-N and L 1641-S (Johnstone & Bally 1999, 2006; Nutter & Ward-Thompson 2007). It is therefore potentially an ideal laboratory for an investigation into the relationship between cores, filaments and outflows. Throughout much of Orion A, one might expect to see flows predominantly orientated east-west.

In Fig. 14c we have plotted a histogram of the jet position angles (in ten degree bins) for all outflows in our sample. The plot suggests a uniform distribution of position angles. Moreover, a Kolmogorov-Smirnov (KS) test shows that there is a >99% probability that such a distribution is drawn from a homogeneously distributed sample. In other words, the position angles of the H_2 flows are completely random. If we consider

only the jets with identified outflow sources a similar situation is found. In this case the probability that the distribution is random is 99.2%. The same also holds if we separate the H_2 jets in the northern region (Dec > -6°), where the dense gas is more tightly constrained to a north-south filament, from those south of the ONC (Dec < -6°). Even for the compact ridge of pre- and proto-stellar cores north of the ONC (OMC 2/3), the outflows are randomly orientated. Similar plots for H_2 jets exceeding an arcminute in length (flows that arguably have more reliable position angles), or for jets with embedded protostars coincident with MAMBO cores, are equally randomly orientated.

So the H_2 jets in Orion A appear to be randomly orientated. Notably, Matthews et al. (2001) and Houde et al. (2004) find that on large scales the field along the integral-shaped filament (north and south of the ONC) is non-uniform. The long axes of the elongated cores along the filament also appear to be randomly orientated (Chini et al. 1997; Johnstone & Bally 1999, 2006; Nutter & Ward-Thompson 2007; see also e.g. Fig. 3). It is therefore not too surprisingly that flow position angles should also be non-uniform. But are the H_2 outflows orientated orthogonal to the cores associated with each outflow source? At 450 pc, the MAMBO beam of $11''$ corresponds to 5×10^3 AU, considerably larger than accretion disk dimensions or the size of the solar system. Even so, many of the cores in Tables 2 and 3 are elongated; if these “circumstellar envelopes” are magnetically tied to the accretion disks they harbour (due to modest ambipolar diffusion), then one might expect them to be orientated perpendicular to the flow axes (Banerjee & Pudritz 2006; Ananthapindika & Whitworth 2008).

In our data, 47 H_2 jet sources are associated with $1200\mu\text{m}$ emission above a surface density $F_{1200} > 75$ mJy. Of these, 42 are associated with cores (rather than “emission” in Tables 2 and 3). From this sample we extract sources where the core major-to-minor axis ratio exceeds 1.3, and exclude very large (diffuse) cores where the Full Width Half Maximum of the Gaussian fit is greater than $50''$ in either axis. We arrive at a sample of just 22 H_2 flows with cores. Surprisingly, even from this finely-tuned sample, the distribution of H_2 jet position angles (PAs) with respect to core PAs is completely random. One might expect that the “longer”, more clearly-defined jets, would be orthogonal to their associated cores. However, in a plot of jet length against “jet-PA minus core-PA” (not shown), even the longest jets seem to be randomly orientated with respect to their progenitor cores.

It seems likely that, in some of the more clustered regions (OMC 2/3, L1641-N, etc.), the MAMBO observations have insufficient resolution to disentangle the molecular envelopes associated with multiple sources. Focusing on a hand-picked sample of sources separate from the main clusters of protostars, sources with well-defined jets and bright, compact cores, is probably necessary. Obviously much higher resolution (sub)mm observations would also be beneficial; ALMA will be useful in this respect.

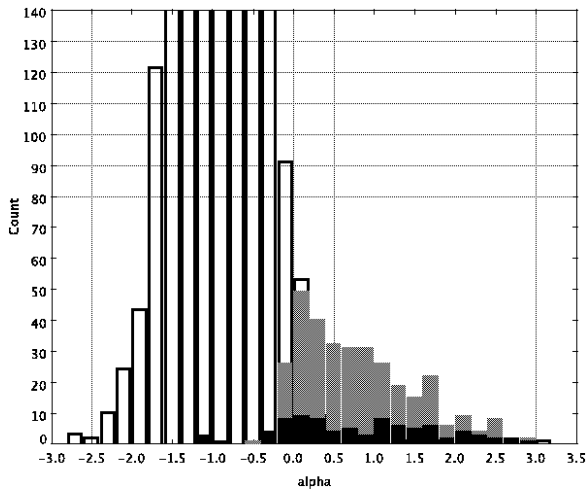


Fig. 17. Histograms showing the number of disk excess sources (open columns), protostars (filled grey columns) and H_2 flow sources (black columns) with a given value of α (in bins of 0.2).

4. Discussion

4.1. Do all protostars drive H_2 outflows?

In Fig. 17 we plot histograms showing the distribution of spectral indices for the Spitzer disk excess sources, the Spitzer protostars, and the outflow sources. As was found to be the case in Perseus (Davis et al. 2008) and the more distant, high mass star forming region, W 75/DR 21 (Davis et al. 2007; Kumar et al. 2007) the majority of H_2 flows are driven by protostars with positive spectral indices. The mean value of α for the disk excess sources, most of which will be T Tauri stars, is -0.85 (std dev = 0.61); for the protostars and the outflow sources, the mean values are 0.80 (std dev = 0.72) and 0.86 (std dev = 0.93); in terms of spectral index, the outflow sources in Orion A appear to be indistinguishable from the protostellar sample.

For the outflow sources in Perseus and DR 21/W 75 the mean values of α are 1.4 and 1.9 , respectively, somewhat higher than in Orion A. The protostellar population in Orion A may therefore be slightly more evolved than in Perseus and DR 21/W 75. Note, however, that the DR 21/W 75 spectral indices were derived from only IRAC photometry, which may result in a higher mean value (the Perseus indices were measured using 2MASS JHK photometry, as well as Spitzer and MIPS data). Also, the larger UV radiation field from the ONC and from B- and A-type stars spread throughout Orion A may accelerate the erosion of protostellar envelopes, thereby reducing measured values of α , although α is largely defined by emission from the inner disk rather than the outer, cold envelope, so this affect may be modest.

The spectral index is clearly a useful tool when searching for H_2 outflow source candidates. Yet of the 290 Spitzer-identified protostars observed in Orion A with WFCAM (excluding the dozen sources in the Orion Nebula), only ~ 84 , or less than one third, seem to be driving outflows that excite H_2

emission. Thus, at first sight it does not appear that all protostars drive H_2 flows.

However, our near-IR images may not be sensitive enough to detect the weakest flows, especially H_2 jets from the least luminous – and least massive – protostars (Caratti O Garatti et al. 2008). Also, the selection criteria used for identifying the Spitzer protostars may well include a handful of background galaxies and AGN (~ 0.7 per square degree), H_2 emission knots, and a number of more evolved young stars. Though faint, heavily reddened Class II sources and disk excess sources viewed edge-on can have the same colours as protostars (Whitney et al. 2003). These classical T Tauri stars rarely produce extensive H_2 flows, because they have either swept away much of their circumstellar environment, or because they occupy regions with a low ambient molecular gas density (they may of course drive HH jets, which our near-IR survey is not sensitive to). Gutermuth et al. (2009) estimate that at most 3.6% of protostars may be edge-on disk excess sources. Our WFCAM images include 1909 disk sources (Megeath et al., in prep.). There may therefore be as many of 70 disk sources in the protostar catalogue that are too evolved to drive H_2 outflows.

The fact that the distributions of α values for the outflow sources and protostars in Fig. 17 are comparable suggests that protostars and H_2 outflow sources are essentially the same objects; as noted earlier, the spread in α for both samples may be due to inclination angle as much as to source age (Whitney et al. 2003; Allen et al. 2004; Megeath et al. 2004). Moreover, there is empirical evidence which suggests that the H_2 outflow phase may be almost as long-lived as the protostellar phase: the dynamical age of an H_2 flow is of the order of 10^4 - 10^5 years (based on a canonical jet length of 1 pc and molecular outflow speeds of 10 - 100 km s^{-1} ; e.g. Arce et al. 2007), while statistical studies indicate that the low mass protostellar phase may last at least as long (Froeblich et al. 2006; Hatchell et al. 2007; Enoch et al. 2008).

Towards the end of the protostellar phase the accretion rate – and therefore the mass loss rate – will evolve quite dramatically, as the source approaches the Class II T Tauri phase. Statistically at least, these sources will probably be associated with mostly atomic, low power jets, which may then persist for timescales of the order of 10^5 – 10^6 years (Reipurth & Bally 2001). Such jets may be undetectable without very deep H_2 imaging, though their sources will in any case usually be identified as “disk excess sources” in the Spitzer analysis used here.

In conclusion, it seems likely that for much of their evolution *all protostars will produce outflows bright in H_2 line emission*. In a sample such as ours, the protostars not associated with H_2 flows may be misclassified disk excess sources, AGN or even H_2 knots. Some protostars may be marginally too evolved or too low mass to produce detectable H_2 jets. Orientation effects and the local, inhomogeneous environment will also play a role in jet detectability.

4.2. Association of H_2 outflow sources with molecular cores

In a recent study, Jørgensen et al. (2007) used a combination of Spitzer IRAC and MIPS photometry and $850\mu\text{m}$ SCUBA observations to identify the youngest protostars in Perseus. They selected 49 MIPS sources that have red [3.6]-[4.5] and/or [8.0]-[24] colours, and are within $15''$ of a SCUBA peak. Davis et al. (2008) later found that most (63% of the reddened MIPS sources they imaged) drive H_2 flows. In Orion A it seems that a similarly high percentage of “protostars with cores” drive molecular (H_2) outflows; note that most of the outflows with identified progenitors in Tables 2 and 3 are associated with discrete $1200\mu\text{m}$ cores.

However, clearly not all molecular cores are associated with H_2 flows. We identify in excess of 500 peaks in the $1200\mu\text{m}$ MAMBO data (Stanke et al., in prep.). Similarly, Nutter & Ward-Thompson (2007) extract almost 400 cores from their more limited $850\mu\text{m}$ SCUBA maps of Orion A. Only about 1/5th of these cores seem to be associated with H_2 outflows. Johnstone & Bally (2006) obtain a similar result in their comparison of SCUBA data with the H_2 images of Sta02; they find that 17 of the 70 SCUBA clumps they identify are clearly associated with H_2 emission.

Many of the cores in Orion A will be prestellar – based on the number of cores without H_2 jets, roughly 80% – which suggests that the H_2 outflow (and therefore protostellar) phase is considerably shorter than the prestellar phase. This statistic assumes that each core produces just one protostar (and H_2 flow), which is almost certainly incorrect; small groups of protostars are often found in each core (see for example the L 1641-N core in Fig. 6). The prestellar phase could therefore be at least an order of magnitude longer than the protostellar/ H_2 outflow phase.

What fraction of *cores containing protostars* drive H_2 flows? In Fig. 18 we plot the entire $1200\mu\text{m}$ map of Orion A. We over-plot the positions of the Spitzer candidate protostars, and mark the locations of the H_2 outflow sources. (Note that the outflow and protostar catalogues are incomplete in the Orion Nebula region; saturation effects, source confusion, and the bright, diffuse nebulosity that pervades the ONC will limit both samples.) Of the 190 protostars in Orion A that were observed with MAMBO, excluding the dozen in the Orion Nebula region, only 70 coincide with $1200\mu\text{m}$ cores (to within an $11''$ radius), although most do coincide with extended and/or diffuse emission. Of these 70 protostars with cores, 43 (61%) appear to be driving molecular H_2 outflows. In some of the less tightly clustered and therefore less complex regions in L 1641, such as the NGC 1980 region in Fig. 5, the number of protostars associated with cores that also drive H_2 jets approaches 100%. Within the limitations of our millimetre and near-IR observations (discussed in the previous section), it seems likely that *most, if not all protostars within molecular cores drive H_2 outflows*. It is also clear that the combination of Spitzer mid-IR photometry and either SCUBA $850\mu\text{m}$ or MAMBO $1200\mu\text{m}$ far-IR photometry is ideal for identifying molecular outflow sources and, in all probability, the youngest protostars.

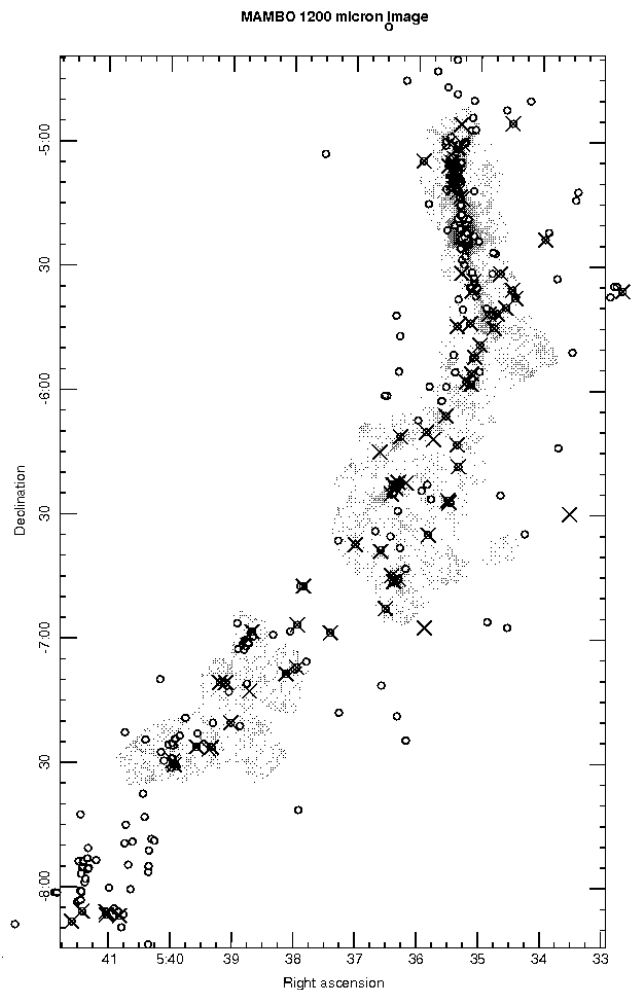


Fig. 18. A logarithmically-scaled image of $1200\mu\text{m}$ emission with, superimposed, the locations of all Spitzer-identified protostars (open circles). H_2 outflow sources are marked with crosses (note that a handful of H_2 jet sources are disk excess sources).

Lastly, we mention that, of the 30 or so protostars in Fig. 18 that are located to the east or west of the edges of the MAMBO map, i.e. beyond the bounds of the high-density molecular ridge that constitutes OMC 2/3 and L 1641, only three protostars are driving H_2 flows. A much larger fraction of protostars within the bounds of the MAMBO map, where ambient gas densities are much higher, are driving molecular outflows. As was noted in the previous section, some of the protostars without H_2 jets may be marginally more evolved; Fig. 18 suggests that these “evolved protostars”, sources close to the Class II T Tauri phase (which may of course drive HH jets), are more widely distributed.

4.3. Clustering and the distribution of protostars and outflow sources.

Qualitatively speaking, if one examines Fig. 18 closely, it appears that *clusters of protostars are not always associated with clusters of H_2 outflows*. In L 1641-C, for example (RA

Table 1. Mean and median Nearest Neighbour (NN) radii for protostars (all sources, sources with H₂ outflows, and sources without) in Orion A. The standard deviation (std) is given in brackets. North and South refer to protostars located north or south of declination -6°, respectively.

Region	5th NN	6th NN	7th NN	10th NN	20th NN
	mean(std)median	mean(std)median	mean(std)median	mean(std)median	mean(std)median
All Protostars	0.087°(0.09°)0.060°	0.097°(0.10°)0.070°	0.106°(0.10°)0.079°	0.13°(0.11°)0.11°	0.20°(0.11°)0.18°
Protostars with flow	0.077°(0.06°)0.064°	0.089°(0.07°)0.085°	0.098°(0.07°)0.096°	0.13°(0.08°)0.12°	0.19°(0.10°)0.20°
Protostars no flow	0.090°(0.10°)0.055°	0.100°(0.11°)0.061°	0.109°(0.11°)0.073°	0.13°(0.12°)0.09°	0.20°(0.12°)0.17°
All Protostars (North)	0.077°(0.08°)0.042°	0.086°(0.09°)0.050°	0.095°(0.10°)0.058°	0.12°(0.11°)0.08°	0.16°(0.12°)0.14°
Protostars with flow (North)	0.059°(0.06°)0.035°	0.068°(0.06°)0.048°	0.075°(0.07°)0.058°	0.10°(0.08°)0.11°	0.14°(0.10°)0.14°
Protostars no flow (North)	0.083°(0.09°)0.047°	0.093°(0.10°)0.051°	0.103°(0.11°)0.059°	0.12°(0.12°)0.08°	0.17°(0.13°)0.13°
All Protostars (South)	0.096°(0.10°)0.075°	0.107°(0.10°)0.094°	0.115°(0.10°)0.101°	0.14°(0.11°)0.12°	0.23°(0.11°)0.21°
Protostars with flow (South)	0.094°(0.06°)0.093°	0.110°(0.06°)0.120°	0.119°(0.06°)0.137°	0.16°(0.07°)0.18°	0.24°(0.06°)0.23°
Protostars no flow (South)	0.097°(0.11°)0.073°	0.106°(0.11°)0.079°	0.114°(0.11°)0.083°	0.14°(0.12°)0.11°	0.23°(0.12°)0.19°

~ 5^h38.7^m, Dec ~ 7°00'; see also Fig. 10), although a dozen protostars and ~30 disk excess sources are identified, there is only one H₂ flow. Likewise, between Re 50 and Haro 4-255 (RA ~ 5^h39.9^m, Dec ~ -7°28'; see also Fig. 12) there is a chain of 16 protostars and at least as many disk excess sources, yet again we only detect three or four molecular H₂ outflows. Neither region is associated with large columns of ambient molecular material (L 1641-C is barely detected in the MAMBO data); the paucity of detected outflows may therefore be due to the evolved nature of the protostars in each region. L 1641-N, on the other hand, is associated with massive dense cores, and a large fraction (roughly 50%) of the protostars power H₂ outflows. Likewise, north of the ONC, in the OMC 2/3 molecular cloud region (between declinations -4°30' and -5°15') where protostars and cores are very highly clustered, there are 65 protostars of which 26 appear to be driving molecular flows (this may be a lower limit, given the abundance of H₂ emission line features, although protostars are also difficult to resolve in this busy, nebulous region).

We also note that regions with multiple H₂ flows often seem to be more sparsely populated with protostars. For example, around HH 1/2 (RA ~ 5^h36.3^m, Dec ~ -6°46'; see also Fig. 8) there are at least half-a-dozen H₂ jets, yet only about the same number of protostars. Similarly, east of HH 1/2 around DFS 123 (Fig. 9) and south of HH 1/2 around HH 38/43/64 (Fig. 10) the ratio of H₂ jets to protostars is roughly one to one, though the number of protostars is again low.

However, neither of the above semi-quantitative observations seems to be related to clustering. We demonstrate this by measuring the radius to the 5th, 6th, 7th, 10th and 20th nearest neighbour (NN) for each of the protostars identified in Orion A. The distribution of 6th NN radii is displayed in Fig. 19, where we distinguish protostars that do drive H₂ flows from those that do not. We also separate protostars north of Dec -6° (the OMC 2/3 region) from those south of Dec -6° (L 1641). In Table 1 we list the mean and median radius for each sample of Nth nearest neighbour radii, and again distinguish outflow sources from the remaining sample of protostars, and contrast the northern region with the south (median values tend to ex-

clude outliers with large radii located on the periphery of each region). Table 1 and Fig. 19 both demonstrate that there is no significant difference between the spatial distribution of protostars that drive H₂ flows and protostars that do not. In other words, the molecular outflow sources are no more – nor no less – clustered than the sources that don't drive H₂ flows. This result is confirmed by K-S testing: for the 6th NN radii, in the northern region there is a 71% probability that the protostar and H₂-outflow-driving source radii are drawn from the same sample; in the south the probability is lower (11%) though still inconclusive – both distributions of NN radii are essentially the same. K-S tests for the 5th and 7th NN radii yield similar results.

We conclude that the differences we note at the beginning of this section are simply due to evolutionary effects. There are clearly regions within Orion A that are more evolved than others; young regions like L 1641-N that contain embedded protostars that drive H₂ outflows, and older regions like L 1641-C with clusters of “protostars” that are not associated with large clouds, dense cores or molecular outflows. The high fraction of H₂-outflow-driving protostars suggests that transition time scales – from protostar with H₂ flow, via protostar without H₂ flow, to disk excess source – are relatively brief. The fact that the protostars without molecular outflows are no more widely distributed (on average) than protostars with outflows suggests that the protostellar phase as a whole is short in comparison to the overall time-scale over which young stars become more widely distributed.

Finally, the NN analysis summarised in Table 1 also demonstrates that there are considerable differences between OMC 2/3 and L 1641. All protostars, regardless of whether they drive H₂ outflows or not, are far more clustered in the north (NN radii are consistently shorter) than in L 1641 in the south. Clustering, the distributions of protostars and disk excess sources, and the population of young stars throughout Orion, will be discussed in detail in a forthcoming paper (Megeath et al., in prep.).

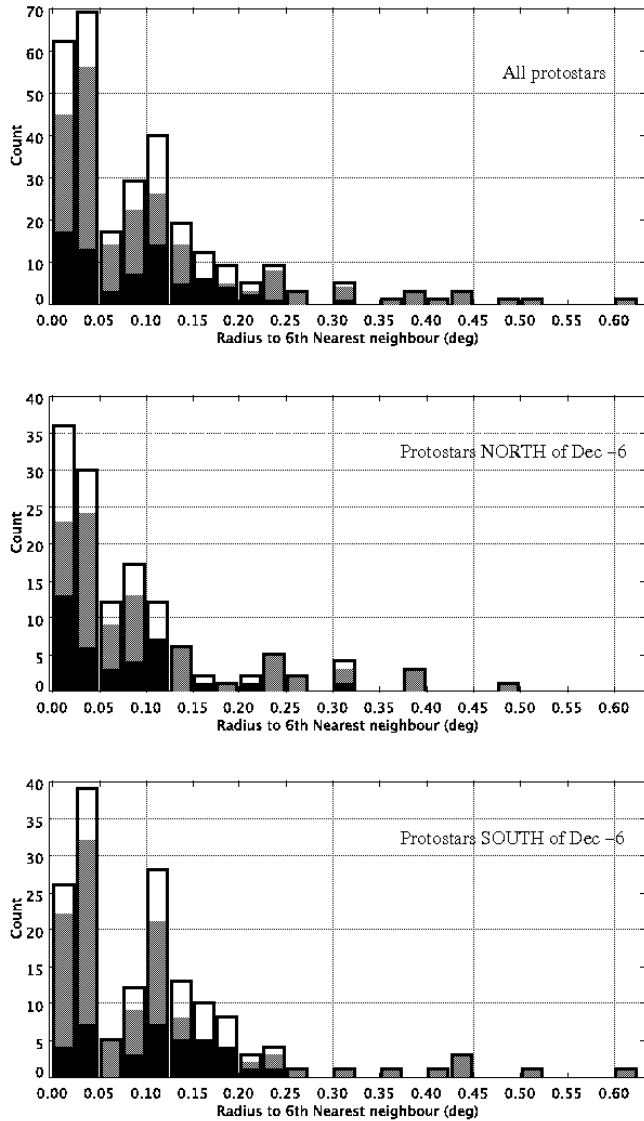


Fig. 19. Histograms showing the distribution of 6th nearest neighbour radii for all Spitzer-identified protostars (open bars), for those that drive H_2 outflows (black filled bars), and for those that do not drive H_2 outflows (grey filled bars). Top - entire region; middle - north of declination -6° ; bottom - south of declination -6° .

5. Summary and Conclusions

We present near-IR images of H_2 outflows spread across an eight square degree region that encompasses most of the Orion A GMC. For much of this region Spitzer photometry is used to identify protostars and disk excess sources, and large-scale (sub)millimetre maps are used to plot the distribution of molecular gas. Tangential velocities (proper motions) are measured for features in 33 outflows; these data are used to help associate the outflows with the protostars and dense molecular cores.

We identify 43 new H_2 outflows, increasing the number of H_2 flows in Orion A to 116 (not including the Orion bullets).

From the Spitzer sample of young stars we find sources for most of these outflows. Of the 300 or so protostars identified by Megeath et al. (in prep.), at least 1/3 seem to be driving H_2 flows. Indeed, the H_2 outflow sources are predominantly protostars (Class 0/I sources) rather than disk excess sources (mostly Class II T Tauri stars), though a few of the latter source sample do seem to power H_2 flows. Most H_2 outflow sources have positive spectral indices and are associated with dust cores; most molecular cores that harbour protostars also drive molecular outflows. All evidence points to the extreme youth of H_2 jet progenitors.

We find no evidence for a preferred molecular outflow direction. Even in OMC 2/3, the region north of the ONC, where the molecular gas is confined to a north-south chain of dense cores, the H_2 flows seem to be randomly orientated. Nor do we find a correlation between H_2 flow length or opening angle and source spectral index or core flux at $1200\mu\text{m}$. We find no evidence that “more evolved” sources, i.e. those with low α or weak $1200\mu\text{m}$ emission, drive longer or less-well-collimated H_2 flows. The caveats associated with measuring flow parameters from H_2 observations are discussed in light of these results.

Finally, we investigate the spatial distribution of H_2 outflow sources in relation to the overall distribution of protostars. Although well-known star clusters, such as L 1641-N and L 1641-C, are associated with clusters of a dozen or so protostars and disk excess sources, only groups or clusters of protostars that are still surrounded by dense molecular gas seem to be associated with multiple H_2 flows. Protostars that power H_2 outflows are no more (nor no less) clustered than protostars that do not. This, together with the fact that a high percentage of protostars do drive H_2 flows, suggests that the H_2 -outflow-driving phase of a protostar’s early evolution is only marginally shorter than the overall lifetime of the protostar; it seems clear that H_2 jets fade very quickly as each source evolves towards the Class II pre-main-sequence phase.

Acknowledgements

We gratefully acknowledge the two referees, Bo Reipurth and John Bally, for their careful reading of the text and very useful comments, which served to improve the accuracy, clarity and overall quality of the paper. Thanks are also due to Dave Nutter for making the SCUBA data available to us. We have made extensive use of the Starlink analysis tools GAIA and TOPCAT (<http://starlink.jach.hawaii.edu/>). We acknowledge the Cambridge Astronomical Survey Unit (CASU) for processing the near-IR data, and the WFCAM Science Archive in Edinburgh for making the bulk of the WFCAM data discussed here available to us. The United Kingdom Infrared Telescope is operated by the Joint Astronomy Centre on behalf of the U.K. Particle Physics and Astronomy Research Council. Some of the WFCAM data reported here were obtained as part of the UKIRT Service Programme. This research made use of data products from the Spitzer Space Telescope Archive. These data products are provided by the services of the Infrared Science Archive operated by the Infrared Processing and Analysis Centre/California Institute of Technology, funded by the National Aeronautics and Space Administration and the

National Science Foundation. We have also made much use of the SIMBAD database, operated at CDS, Strasbourg, France.

References

- Allen L.E. et al., 2004, *ApJS*, 154, 363
- Allen L.E., Davis C.J., 2008, in *Handbook of Star Forming Regions Vol I*, ed. B. Reipurth, ASP Monographs, p.621
- Anathpindika S., Whitworth A.P., 2008, *A&A*, 487, 605
- Anglada G., Villuendas E., Estalella R., Beltrán M.T., Rodríguez L.F., Torrelles J.M., Curiel S., 1998, *AJ*, 116, 2953
- Antonucci S., Nisini B., Giannini T., Lorenzetti D., 2008, *A&A*, 479, 503
- Arce H.A., Sargent A.I., 2006, *ApJ*, 646, 1070
- Arce H.A., Shepherd D., Gueth F., Lee C.F., Bachiller R., Rosen A., Beuther H., 2007, in *Protostars and Planets V*, eds. B. Reipurth, D. Jewitt, p.245
- Aspin C.A., Reipurth B., *MNRAS*, 311, 522
- Bally J., Devine D., 2001, *ApJ*, 546, 299
- Bally J., Heathcote S., Reipurth B., Morse J., Hartigan P., Schwartz R., 2002, *AJ*, 123, 2627
- Bally J., O'Dell C.R., McCaughrean M.J., 2000, *AJ*, 119, 2919
- Banerjee & Pudritz 2006, *ApJ*, 641, 949
- Beck T.L., 2007, *AJ*, 133, 1689
- Caratti O Garatti A., Froebrich D., Eislöffel J., Giannini T., Nisini B., 2008, *A&A*, 485, 137
- Carpenter J.M., Hillenbrand L.A., Skrutskie M.F., 2001, *AJ*, 121, 3160
- Casali M., et al., 2007, *A&A*, 467, 777
- Cavanagh B., Hirst P., Jenness T., Economou F., Currie M.J., Todd S., Ryder S.D., 2003, *ASPC*, 295, 237
- Chini R., Reipurth B., Ward-Thompson D., Bally J., Nyman L.-ø., Sievers A., Billawala Y. 1997, *ApJ*, 474, L135
- Crutcher R.M., Troland T.H., Lazareff B., Paubert G., Kazés I., 1999, *ApJ*, 514, L121
- Davis C.J., Kumar M.S.N., Sandell G., Froebrich D., Smith M.D., Currie M.J., 2007, *MNRAS*, 374, 29
- Davis C.J., Eislöffel J., Ray T.P., 1994, *ApJ*, 426, L93
- Davis C.J., Dent W.R.F., Matthews H.E., Coulson I.M., McCaughrean M.J., 2000, *MNRAS* 318, 952
- Davis C.J., Scholz P., Lucas P.W., Adamson A., 2008, *MNRAS*, 387, 954
- Devine D., Bally J., Reipurth B., Heathcote S., 1997, *AJ*, 114, 2095
- Doppmann G.W., Greene T.P., Covey K.R., Lada C.J., 2005, *AJ*, 130, 1145
- Doppmann G.W., Jaffe D.T., White R.J., 2003, *AJ*, 126, 3042
- Dye S., et al., 2006, *MNRAS*, 372, 1227
- Eislöffel J., Mundt R., Böhm K.-H., 1994, *AJ*, 108, 1042
- Eislöffel J., Mundt R., 1997, *AJ*, 114, 280
- Enoch M.L., Evans N.J., Sargent A.I., Glenn J., Rosolowsky E., Myers P., 2008, *ApJ*, 684, 1240
- Fazio G.G., et al., 2004 *ApJS*, 154, 10
- Froebrich D.F., Schmeja S., Smith M.D., Klessen R.S., 2006, *MNRAS*, 368, 435
- Gålfalk M., Olofsson G., 2007, *A&A*, 466, 579
- Greene T.P., Lada C.J., 2002, *AJ*, 124, 2185
- Gutermuth R.A., Myers P.C., Megeath S.T., Allen L.E., Pipher J.L., Muzerolle J., Porras A., Winston E., Fazio G., 2008, *ApJ*, 674, 336
- Gutermuth R.A., Megeath S.T., Myers P.C., Allen L.E., Pipher J.L., Fazio G.G., 2009, *ApJS*, submitted
- Hatchell J., Fuller G.A., Richer J.S., Harries T.J., Ladd, E.F., 2007, *A&A*, 468, 1009
- Hester J.J., Stapelfeldt K.R., Scowen P.A., 1998, *AJ*, 116, 372
- Hewett P.C., Warren S.J., Leggett S.K., Hodgkin S.T., 2006, *MNRAS*, 367, 454
- Heyer M.H., Strom S.E., Strom K.M., 1987, *AJ*, 94, 1653
- Houde M, Dowell C. D., Hildebrand, R.H., Dotson J.L., Vaillancourt J.E., Phillips T.G., Peng R., Bastien P., 2004, *ApJ*, 604, 717
- Kreysa E. et al. 1999, *Infrared Physics and Technology*, 40, 191
- Johnstone D., Bally J., 1999, *ApJ*, 510, L49
- Johnstone D., Bally J., 2006, *ApJ*, 653, 383
- Jørgensen J.K. et al. 2007, *ApJ*, 656, 293
- Kassis M., Adams J.D., Campbell M.F., Deutsch L.K., Hora J.L., Jackson J.M., Tollestrup E.V., 2006, *ApJ*, 637, 823
- Kumar M.S.N, Davis C.J., Grave J.M.C., Ferreira B., Froebrich D., 2007, *MNRAS*, 374, 54
- Kutner M.L., Tucker K.D., Chin G., Thaddeus P., 1977, *ApJ*, 215, 521
- Larry K, 2008, *ApJ*, in press
- Lee J.-K., Burton M.G., 2000, *MNRAS*, 315, 11
- Lee C.-F., Mundy L.G., Stone J.M., Ostriker E.C., 2002, *ApJ*, 576, 294
- Matthews B.C., Fiege J.D., Moriarty-Schieven, G., 2002, *ApJ*, 569, 304
- Matthews B.C., Wilson C.D., Fiege J.D., 2001, *ApJ*, 562, 400
- Megeath S.T. et al., 2004, *ApJS*, 154, 367
- Megeath S.T., Allgaier E., Young E., Allen T., Pipher J.L., Wilson T.L., 2009, *AJ*, submitted
- Ménard F., Duchéne, G. 2004, *Ap&SS*, 292, 419
- Mouschovias T., 1976, *ApJ*, 207, 141
- Nutter D., Ward-Thompson D., 2007, *MNRAS*, 374, 1413
- Peterson D., Megeath S.T., 2008, in *Handbook of Star Forming Regions Vol I*, ed. B. Reipurth, ASP Monographs, p.590
- Reipurth B., 1985, *A&AS*, 61, 319
- Reipurth B., 1989, *A&A*, 220, 249
- Reipurth B., Bally J., 2001, *ARA&A*, 39, 403
- Reipurth B., Bally J., Devine D., 1997, *AJ*, 114, 2708
- Reipurth B., Devine D., Bally J., 1998, *AJ*, 116, 1396
- Reipurth B., Heathcote S., Yu K.C., Bally J., Rodríguez L.F., 2000, *ApJ*, 534, 317
- Rieke G.H., et al. 2004, *ApJSS*, 154, 25
- Sakamoto S., Hayashi M., Hasegawa T., Handa T., Oka T., 1994, *ApJ*, 425, 641
- Schild H., Miller S., Tennyson J., 1997, *A&A*, 318, 608
- Simpson J.P., Colgan S.W.J., Erickson E.F., Burton M.G., Schultz A.S.B., 2006, *ApJ*, 642, 339
- Slesnick C.L., Hillenbrand L.A., Carpenter J.M., 2004, *ApJ*, 610, 1045
- Smith M.D., Rosen A., 2005, *MNRAS*, 357, 1370
- Stanke T., 2000, Ph.D. Thesis, Universität Potsdam
- Stanke T., McCaughrean M.J., Zinnecker H., 2002, *A&A*, 392, 239 (Sta02)
- Stanke T., Williams, J.P. 2007, *AJ*, 133, 1320
- Strom K.M., Strom S.E., Wolf S.C., Morgan J., Wenz M., 1986, *ApJS*, 62, 39
- Tamura M., et al. 2006, *ApJ*, 649, L29
- Usuda T., Sugai H., Kawabata H., Inoue M.Y., Katata H., Tanaka M., 1996, *ApJ*, 464, 818
- Yu K.C., Bally J., Devine D., 1997, *ApJ*, 485, L45
- Yu K.C., Billawala Y., Smith M.D., Bally J., Butner H.M., 2000, *AJ*, 120, 1974
- Vallée J.P., Fiege J.D., 2006, *ApJ*, 636, 332
- Velusamy T., Langer W.D., Marsh K.A., 2007, *ApJ*, 668, L159
- Whitney B. A., Indebetouw R.; Bjorkman J.E., Wood K., 2004, *ApJ*, 617, 1177
- Whitney B.A., Wood K., Bjorkman J.E., Cohen M., 2003, *ApJ* 598, 1079
- Williams J.P., Plambeck R.L., Heyer M.H., 2003, *ApJ*, 591, 1025

Table 2. H₂ jets and outflows in Orion A, from the catalogue of Sta02.

SMZ	RA ^a (J2000)	Dec ^a (J2000)	Outflow ^b source	α^b	850 μm^c peak	A_{p850}^c (arcsec)	I_{850}^c (Jy)	F_{850}^c (Jy/bm)	1200 μm^d peak	A_{p1200}^d (")	I_{1200}^d (Jy)	F_{1200}^d (Jy/bm)	L^e (')	θ^e (deg)	PA ^e (deg)	HH ^f
1	5:35:19.3	-4:55:45	IRS 1	-0.27	no obs	–	–	–	undetected	–	–	–	0.3	20	68	–
2	5:35:31.6	-5:00:14	IRS 2	-1.04	undetected	–	–	–	undetected	–	–	–	0.4	–	140	–
3	5:35:18.3	-5:00:33	IRS 3	0.31	AN-535182-50021	19x14	5.9	2.13	MMS 3	22x14(92)	0.48	0.57	5.2	30	85	–
4	5:35:23.5	-5:01:29	IRS 4	2.35	AN-535235-50132	21x16	9.7	6.23	MMS 4	137x50(147)	4.64	1.93	0.5	–	170	–
5	5:35:22.4	-5:01:14	IRS 5	2.90	AN-535224-50114	13x10	3.9	2.60	MMS 5	14x13(150)	2.07	0.52	0.6	50	90	293
6	5:35:26.6	-5:03:55	IRS 6	1.53	AN-535265-50356	37x28	6.5	1.63	MMS 6	27x23(163)	2.22	0.31	13	–	85	294/295
7	5:35:28.0	-5:04:58	IRS 7	1.04	AN-535274-50511	32x23	5.3	0.44	MMS 7	35x16(136)	0.44	0.12	~6	10	30	–
8	(5:35:42.1	-5:04:39)	?	–	?	–	–	–	?	–	–	–	–	–	–	–
9	5:35:25.8	-5:05:44	IRS 9	1.54	AN-535258-50551	38x22	6.3	1.55	MMS 9	35x20(50)	1.31	0.24	2.8	42	80	330
10	5:35:31.5	-5:05:47	IRS 10	-0.12	AN-535324-50547	50x28	5.3	0.42	MMS 10	44x31(27)	2.22	0.12	1.5	15	50	287
11/13	5:35:23.3	-5:07:10	IRS 11	0.17	AN-535236-50711	16x13	2.5	1.11	MMS 11	31x18(122)	1.08	0.20	~1	–	~20	–
12	5:35:27.7	-5:07:04	IRS 12	1.85	AN-535279-50711	18x14	0.8	0.24	MMS 12	29x23(173)	0.54	0.11	0.3	–	8	–
14/16	5:35:25.6	-5:07:57	IRS 14	0.93	emission	–	–	0.43	MMS 14	20x15(47)	0.27	0.06	~4	35	40	383
15	5:35:22.4	-5:08:05	IRS 15	-0.10	AN-535222-50817	18x14	1.2	0.38	MMS 15	20x15(98)	0.29	0.09	0.4	–	~45	385
17	5:35:27.0	-5:09:54	IRS 17?	0.54	emission	–	–	5.80	MMS 17	25x22(41)	6.06	1.07	1.8	50	25	887
18	(5:35:29.6	-5:08:58)	?	–	?	–	–	–	?	–	–	–	–	50	–	–
19	5:35:26.8	-5:09:25	IRS 19	-0.03	emission	–	–	1.90	MMS 19	20x15(92)	0.87	0.28	0.5	–	100	384
20	5:35:25.7	-5:09:49	IRS 20	0.14	emission	–	–	1.45	emission	–	–	0.36	0.7	–	175	–
21/22	5:35:26.9	-5:11:07	IRS 21	-1.01	emission	–	–	0.33	emission	–	–	0.10	1.6	–	175	–
23	5:35:24.7	-5:10:30	IRS 23	1.18	emission	–	–	0.53	MMS 23	20x16(175)	0.48	0.18	~4	–	17	–
24	5:35:23.3	-5:12:03	IRS 24	1.37	AN-535234-51205	21x16	3.2	1.28	MMS 24	16x12(174)	0.44	0.35	1.5	27	61	536
25	5:35:20.1	-5:13:16	IRS 25	0.04	emission	–	–	0.87	MMS 25	23x12(126)	0.65	0.29	3.0	–	160	44/535
26	(5:35:10.9	-5:23:12)	?	–	?	–	–	–	?	–	–	–	2.6	–	125	–
27	(5:35:11.6	-5:23:41)	?	–	?	–	–	–	?	–	–	–	–	–	–	510?
28	(5:35:10.9	-5:23:46)	?	–	?	–	–	–	?	–	–	–	–	–	–	510?
29	5:34:40.9	-5:31:44	IRS 29	1.47	no obs	–	–	–	MMS 29	21x16(160)	0.42	0.16	5.0	20	156	–
30	5:35:18.3	-5:31:42	IRS 30	-0.36	undetected	–	–	–	MMS 30	18x17(64)	0.06	0.03	0.9	–	25	540
31	5:34:35.5	-5:39:59	IRS 31	1.01	no obs	–	–	–	MMS 31	33x25(22)	0.26	0.06	0.9	60	150	–
32	(5:35:11.4	-5:39:38)	?	–	?	–	–	–	?	–	–	–	0.8	–	170	–
33	5:34:51.9	-5:41:33	IRS 33?	1.64	undetected	–	–	–	undetected	–	–	–	0.5	–	134	–
34	5:35:09.9	-5:43:45	IRS 34	1.54	undetected	–	–	–	undetected	–	–	–	–	–	–	–
35	5:34:46.9	-5:44:51	IRS 35?	0.73	undetected	–	–	–	undetected	–	–	–	1.0	–	58	–
36	(5:35:10.0	-5:45:06)	?	–	?	–	–	–	?	–	–	–	–	–	–	–
37	5:35:05.5	-5:51:54	IRS 37	0.77	no obs	–	–	–	undetected	–	–	–	–	–	–	–
38	5:35:08.6	-5:55:54	IRS 38	1.80	no obs	–	–	–	MMS 38	19x15(121)	0.88	0.31	~7	10	~150	–
39	5:35:09.0	-5:58:28	IRS 39	1.06	emission	–	–	0.41	MMS 39	19x15(155)	0.54	0.17	>3	20	~30	–
40	5:35:33.2	-6:06:10	IRS 40?	0.46	emission	–	–	–	undetected	–	–	–	3.8	–	16	–
41	5:35:13.4	-5:57:58	IRS 41	2.30	no obs	–	–	–	MMS 41	19x14(153)	0.79	0.21	6.0	–	9	–
42	5:35:22.2	-6:13:06	IRS 42	1.21	AS-535213-61313	26x17	0.7	0.14	MMS 42	57x37(35)	0.88	0.06	5.0	12	69	–
43	5:35:52.0	-6:10:02	IRS 43	0.37	AS-535524-61007	33x19	1.3	0.49	MMS 43	22x16(150)	0.58	0.19	~2	–	~45	–
44	5:35:45.2	-6:11:44	IRS 44?	-1.19	undetected	–	–	–	undetected	–	–	–	1.3	–	132	–
45	5:36:17.3	-6:11:11	IRS 45	0.93	undetected	–	–	–	MMS 45	32x22(166)	0.22	0.04	2.3	60	3	–

Davis et al.: A census of molecular hydrogen outflows and their sources along the Orion A molecular ridge

46	5:36:37.0	-6:14:58	IRS 46	0.51	AS-536366-61459	19x13	0.8	0.30	MMS 46	29x20(128)	0.52	0.11	~0.5	-	~0	304
47	(5:35:38.1	-6:15:08)	?	-	?	-	-	-	?	-	-	-	0.9	-	155	-
48	5:36:10.5	-6:19:55	?	-	?	-	-	-	?	-	-	-	1.4	-	40	299
49	5:36:19.5	-6:22:12	IRS 49	0.79	AS-536196-62209	77x44	15.8	1.92	MMS 49	20x9(88)	0.16	0.53	~34	-	175	303
50	5:36:11.5	-6:22:22	IRS 50?	-0.90	undetected	-	-	-	undetected	-	-	-	2.0	-	~170	-
51	5:36:24.6	-6:22:41	IRS 51	1.23	AS-536250-62241	49x27	3.1	0.59	MMS 51	52x24(155)	1.39	0.12	>4.0	40	69	301
52	(5:36:39.1	-6:22:38)	?	-	?	-	-	-	?	-	-	-	-	-	-	-
53	5:36:18.8	-6:22:10	IRS 53	2.47	AS-536196-62209	77x44	15.8	3.72	MMS 53	17x16(38)	3.09	1.01	0.6	-	45	-
54	(5:36:31.0	-6:24:49)	?	-	?	-	-	-	?	-	-	-	-	-	-	-
55	5:35:29.8	-6:26:59	IRS 55	1.77	AS-535297-62701	27x19	1.7	0.83	MMS 55	14x13(4)	1.92	0.26	17	-	165	34
56	5:35:30.9	-6:26:32	IRS 56	1.16	AS-535305-62622	32x21	1.6	0.26	MMS 56	54x38(168)	1.34	0.09	1.8	4	8	-
57	(5:36:56.9	-6:34:17)	?	-	?	-	-	-	?	-	-	-	-	-	-	292
58	5:37:00.5	-6:37:11	IRS 58	-0.16	AS-537004-63715	36x19	1.5	0.44	MMS 58	63x38(179)	2.22	0.15	4.0	12	60	-
59	5:36:36.1	-6:38:52	V380 Ori-NE	-	AS-536361-63857	38x18	1.8	0.93	MMS 59	38x18(167)	1.62	0.35	2.0	18	~0	-
60	(5:36:22.0	-6:41:42)	?	-	?	-	-	-	?	-	-	-	-	-	-	35
61	5:36:18.9	-6:45:23	IRS 61?	2.07	emission	-	-	0.88	emission	-	-	0.25	~3.6	-	~165	-
62	(5:36:11.6	-6:43:04)	?	-	?	-	-	-	?	-	-	-	-	-	-	3
63	5:36:25.1	-6:44:42	IRS 63	0.04	AS-536259-64440	38x27	2.2	0.47	MMS 63	58x48(20)	2.91	0.17	0.5	36	~45	147
64	5:36:22.8	-6:46:06	HH 1/2-VLA	-	AS-536229-64618	52x30	6.2	1.36	MMS 64	42x27(25)	5.61	0.42	>3	32	~145	1/2
65	(5:36:21.2	-6:46:08)	?	-	?	-	-	-	-	-	-	-	1.9	-	110	144
66	5:38:40.5	-6:58:22	IRS 66	-0.04	no obs	-	-	-	MMS 66	13x13(168)	0.93	0.19	2.6	4	130	-
67	5:37:57.0	-7:06:56	IRS 67	2.07	no obs	-	-	-	MMS 67	22x20(98)	0.79	0.14	16	18	126	38/43/64
68	5:38:07.5	-7:08:29	IRS 68	0.25	no obs	-	-	-	MMS 68	24x17(2)	0.12	0.02	1.2	10	130	-
69	5:39:05.8	-7:10:39	IRS 69	2.63	no obs	-	-	-	undetected	-	-	-	~0.4	-	90	-
70	5:38:42.8	-7:12:44	IRS 70	-0.23	no obs	-	-	-	MMS 70	15x11(145)	0.07	0.04	~1.7	30	~135	449
71	5:39:00.9	-7:20:23	IRS 71	1.55	no obs	-	-	-	MMS 71	65x31(173)	0.40	0.01	0.9	-	128	-
72	5:39:19.6	-7:26:19	IRS 72b	0.33	no obs	-	-	-	MMS 72	22x20(176)	3.17	0.30	5.4	70	65	469
73	5:39:22.3	-7:26:45	IRS 73	-0.37	no obs	-	-	-	MMS 73	15x10(24)	0.34	0.09	2.3	14	133	470
74	(5:40:23.7	-7:20:32)	?	-	no obs	-	-	-	?	-	-	-	>1.0	-	53	-
75	(5:40:25.8	-7:22:14)	?	-	no obs	-	-	-	?	-	-	-	>1.5	-	45	-
76	5:39:55.9	-7:30:28	IRS 76	2.70	no obs	-	-	-	MMS 76	16x15(117)	2.62	0.55	14	-	~60	65

^a Position of the H₂ outflow source if one is listed in column 4. Otherwise, the position of the brightest knot in the flow is given (enclosed in brackets). Note that the well-known sources of the HH 1/2, HH 83 and V380-Ori-NE flows were not identified in our tables of Spitzer protostars or disk excess sources.

^b Most likely H₂ outflow source from the Spitzer photometry together with the spectral index, α . Just a question mark means there is no obvious H₂ flow source candidate.

^c 850 μ m dust core coincident with the H₂ outflow source (from Nutter & Ward-Thompson 2007). The source must lie within a 14'' radius (the JCMT beam at 850 μ m) of the core position given by Nutter & Ward-Thompson in their Table A1. "Emission" or "undetected" means that no core appears in their table. However, "emission" means that the source identified in column 4 is associated with diffuse 850 μ m emission (surface brightness >100 mJy beam⁻¹, which is roughly equivalent to 5 σ); a question mark means there are cores (or emission) in the vicinity which could be associated with the outflow or its source; "no obs" means that the outflow is outside the bounds of the SCUBA map. The core size (major/minor axis dimensions), Ap_{850} , and integrated flux, I_{850} , are given for each core; F_{850} is the flux, in Jy beam⁻¹, measured towards each IRS source (not necessarily the peak flux of the associated core).

^d Same as for the 850 μ m cores, but for cores identified from our analysis of the 1200 μ m observations of Stanke et al. (in prep.). In this case the source must lie within 11'' of the core centroid; "emission" corresponds to a surface brightness >75 mJy beam⁻¹ ($\sim 5\sigma$). The values given in brackets in the Ap_{1200} column are the orientation of the core major axis (this information was not available for the 850 μ m cores).

^e Entire length (L) of all H₂ knots (in both lobes), or the distance from the source to the most distant H₂ knot if only one flow lobe is identified; opening angle (θ) measured from a cone centred on the outflow source that includes all H₂ features in the flow; position angle (PA) measured east of north.

^f Associated HH objects, if any are known.

Table 3. New H₂ jets in Orion A (additions to the catalogue of Sta02). Columns are the same as for Table 2.

DFS	RA ^a (J2000)	Dec ^a (J2000)	Outflow ^b source	α^b	850 μm^c peak	A_{p850}^c (arcsec)	I_{850}^c (Jy)	F_{850}^c (Jy/bm)	1200 μm^d peak	A_{p1200}^d (")	I_{1200}^d (Jy)	F_{1200}^d (Jy/bm)	L^e (')	θ^e (deg)	PA ^e (deg)	HH ^f
101	5:34:29.5	-4:55:31	IRS 101	1.37	no obs	–	–	–	no obs	–	–	–	5.3	–	~160	–
102	5:35:55.7	-5:04:38	IRS 102	0.04	undetected	–	–	–	no obs	–	–	–	>3.5	9	~90	42
103	5:35:24.3	-5:08:31	IRS 103	1.18	AN-535245-50832	26x16	4.3	1.55	MMS 103	21x16(178)	1.06	0.35	0.2	40	~170	–
104	5:35:18.5	-5:13:38	IRS 104	-0.05	AN-535183-51338	13x8	0.3	0.07	MMS 104	18x12(180)	0.12	0.10	0.25	–	135	–
105	5:33:57.4	-5:23:30	IRS 105	2.34	no obs	–	–	–	no obs	–	–	–	1.7	30	11	–
106	5:34:29.4	-5:35:43	IRS 106	1.78	no obs	–	–	–	MMS 106	109x20(160)	0.31	0.01	~0.5	–	~10	–
107	5:34:26.4	-5:37:41	IRS 107	0.06	no obs	–	–	–	undetected	–	–	–	1.5	3	95	–
108	5:35:06.5	-5:33:35	IRS 108?	0.43	emission	–	–	0.16	MMS 108	18x7(114)	0.07	0.08	0.5	–	~95	541/882
109	5:35:08.5	-5:35:59	IRS 109	1.21	AN-535082-53558	34x25	3.3	0.88	MMS 109	74x45(20)	4.83	0.19	4.7	5	93	–
110	5:32:42.5	-5:35:55	IRS 110	0.87	no obs	–	–	–	no obs	–	–	–	–	–	–	–
111	5:34:44.1	-5:41:26	IRS 111?	2.10	AS-534439-54128	21x20	0.8	0.28	MMS 111	34x28(115)	0.71	0.09	0.8	25	~50	–
112	5:35:22.6	-5:44:30	IRS 112	0.26	undetected	–	–	–	undetected	–	–	–	3.0	4	105	–
113	5:35:00.5	-5:49:02	IRS 113?	0.61	no obs	–	–	–	undetected	–	–	–	3.7	11	5	–
114	(5:32:22.0	-5:34:52)	?	–	no obs	–	–	–	no obs	–	–	–	–	–	–	–
115	5:36:25.9	-6:24:58	IRS 115	0.13	emission	–	–	0.73	emission	–	–	0.20	>1.2	10	~60	–
116	5:35:20.9	-6:18:22	IRS 116?	0.18	undetected	–	–	–	undetected	–	–	–	1.3	29	133	33/40
117	5:33:32.5	-6:29:44	HH 83-IRS	–	no obs	–	–	–	no obs	–	–	–	10.8	6	108	83/84
118	5:36:21.8	-6:23:30	IRS 118	-0.08	AS-536220-62325	19x17	0.6	0.29	MMS 118	15x11(89)	0.17	0.11	0.35	35	165	–
119	5:35:50.0	-6:34:53	IRS 119	1.37	emission	–	–	0.16	undetected	–	–	–	~0.1	–	~80	–
120	(5:37:47.0	-6:53:33)	?	–	no obs	–	–	–	no obs	–	–	–	~0.1	–	~120	–
121	5:36:23.5	-6:46:15	IRS 121	0.79	AS-536229-64618	52x30	6.2	0.96	MMS 121	41x27(25)	5.61	0.25	6.0	4	71	36
122	5:37:51.0	-6:47:20	IRS 122	1.07	no obs	–	–	–	no obs	–	–	–	3.0	33	142	89
123	(5:37:33.1	-6:50:20)	?	–	no obs	–	–	–	no obs	–	–	–	8.5	30	~95	–
124	5:36:31.0	-6:52:41	IRS 124	0.39	no obs	–	–	–	undetected	–	–	–	1.0	39	~140	–
125	(5:35:53.2	-6:57:13)	no obs	–	no obs	–	–	–	no obs	–	–	–	3.7	–	~15	127
126	5:37:24.5	-6:58:33	IRS 126	-0.02	no obs	–	–	–	no obs	–	–	–	5.6	6	120	–
127	5:37:56.6	-6:56:39	IRS 127	2.02	no obs	–	–	–	no obs	–	–	–	~0.1	40	~90	–
128	(5:37:59.0	-7:13:15)	?	–	no obs	–	–	–	?	–	–	–	–	–	–	–
129	5:39:11.9	-7:10:35	IRS 129	0.25	no obs	–	–	–	MMS 129	59x35(154)	1.04	0.03	~0.8	–	~140	–
130	(5:40:10.6	-7:10:46)	?	–	no obs	–	–	–	?	–	–	–	1.0	–	150	–
131	5:39:57.4	-7:29:33	IRS 131	2.40	no obs	–	–	–	MMS 131	36x22(152)	0.88	0.13	6.5	–	73	–
132	(5:39:10.3	-7:39:39)	?	–	no obs	–	–	–	?	–	–	–	~20	15	~60	–
133	5:39:34.3	-7:26:11	IRS 133?	0.06	no obs	–	–	–	undetected	–	–	–	~9.5	9	170	–
134	(5:41:06.2	-8:00:14)	?	–	no obs	–	–	–	no obs	–	–	–	>0.5	–	~35	–
135	(5:40:46.4	-8:04:36)	?	–	no obs	–	–	–	no obs	–	–	–	2.5	–	90	–
136	5:41:02.0	-8:06:02	IRS 136	1.18	no obs	–	–	–	no obs	–	–	–	1.5	12	115	–
137	5:41:01.7	-8:06:45	IRS 137	1.64	no obs	–	–	–	no obs	–	–	–	1.5	15	60	–
138	5:40:48.8	-8:06:57	IRS 138	1.99	no obs	–	–	–	no obs	–	–	–	13.4	45	130	–
139	(5:41:23.9	-8:12:47)	?	–	no obs	–	–	–	no obs	–	–	–	~0.5	–	~80	–
140	(5:42:31.9	-8:01:14)	?	–	no obs	–	–	–	no obs	–	–	–	–	–	–	–
141	5:41:25.3	-8:05:55	IRS 141	0.29	no obs	–	–	–	no obs	–	–	–	0.5	28	90	–
142	(5:39:42.4	-8:02:58)	?	–	no obs	–	–	–	no obs	–	–	–	–	–	–	–
143	5:41:35.4	-8:08:22	IRS 143	1.64	no obs	–	–	–	no obs	–	–	–	~5	–	~160	–

Appendix A: Description of the H₂ outflows in Orion A

For a description of the new DFS outflows, and images of each flow, please visit <http://www.jach.hawaii.edu/~cdavis/>

Appendix B: Proper motion measurements

For a description of the proper motion measurements and images of each flow with PM vectors superimposed, please visit <http://www.jach.hawaii.edu/~cdavis/>

This figure "davis-fg2.jpg" is available in "jpg" format from:

<http://arxiv.org/ps/0812.3733v1>